Succination of Dihydrolipoyllysine Succinyltransferase by Fumarate Exacerbates Defective Mitochondrial ATP Production during Complex I Deficiency

Gerardo G. Piroli[1], Richard S. McCain [1], Allison M. Manuel[1], Holland H. Smith[1], William E. Cotham[2], Michael D. Walla[2], and Norma Frizzell[1,*]

[1] Department of Pharmacology, Physiology & Neuroscience, School of Medicine, University of South Carolina, Columbia, SC 29209, USA

[2] Mass Spectrometry Center, Department of Chemistry & Biochemistry, University of South Carolina, Columbia, SC 29205, USA

* Lead contact, and to whom correspondence should be addressed: Norma Frizzell, Department of Pharmacology, Physiology & Neuroscience, School of Medicine, University of South Carolina, 6439 Garners Ferry Road, Columbia, SC 29209, USA, Tel.: (803) 216-3521; Fax: (803) 216-3538; Email: norma.frizzell@uscmed.sc.edu

Summary

The *NDUFS4* knockout (KO) mouse phenotype resembles the human Complex I deficiency Leigh Syndrome. The irreversible succination of protein thiols by fumarate is increased in select regions of the *NDUFS4* KO brain affected by neurodegeneration, suggesting a mechanistic role in neurodegenerative decline. We report that dihydrolipoyllysine-residue succinyltransferase (DLST), a component of the α-ketoglutarate dehydrogenase complex (KGDHC) of the tricarboxylic acid (TCA) cycle, is succinated in the *NDUFS4* KO brain. Succination of DLST reduced KGDHC activity in the brainstem (BS) and olfactory bulb (OB) of KO mice. The defective production of KGDHC derived succinyl-CoA resulted in decreased mitochondrial substrate level phosphorylation, further aggravating the OXPHOS ATP deficit. Protein succinylation, an acylation modification that requires succinyl-CoA, was reduced in the KO mice. Our data demonstrate that the biochemical deficit extends beyond impaired Complex I assembly and OXPHOS deficiency, functionally impairing select components of the TCA cycle to drive metabolic perturbations in affected neurons.

Keywords

Fumarate, chemical modification, succination, mitochondria, Leigh Syndrome, Complex I, dihydrolipoyllysine succinyltransferase, substrate level phosphorylation

Highlights

- Cysteine succination by fumarate is increased in model of Complex I deficiency
- Succination of DLST impairs KGDHC activity, limits SLP, and reduces lysine succinylation
- Irreversible succination drives neuropathology independent of the bioenergetic defect

Introduction

Leigh syndrome is a mitochondrial disease predominantly caused by single gene defects in the oxidative phosphorylation (OXPHOS) machinery or the pyruvate dehydrogenase complex. It is characterized by bilateral necrotizing lesions of the basal ganglia and brainstem (BS), lactic acidosis, ataxia, seizures, and respiratory failure (Lake et al., 2016). Leigh syndrome is associated with mutations in at least 23 genes that lead to mitochondrial Complex I deficiency (Lake et al., 2016), with mutations in *NDUFS4*, a gene that encodes the small assembly protein NADH dehydrogenase (ubiquinone) iron-sulfur protein 4 (Ndufs4) (Calvaruso et al., 2011; Ortigoza-Escobar et al., 2016), among the most frequent.

The homozygous *NDUFS4* knockout mouse (Ndufs4 KO) recapitulates many biochemical and clinical aspects of Leigh syndrome, including lactic acidosis, BS degeneration, motor retardation and fatal respiratory failure at 8 weeks after birth; the neuropathology also extends to the olfactory bulb (OB) and some cerebellar nuclei (Kruse et al., 2008; Quintana et al., 2010). Selective deletion of Ndufs4 in glutamatergic neurons leads to BS inflammation, motor and respiratory deficits and early death; whereas ablation of Ndufs4 in GABAergic neurons causes basal ganglia inflammation, hypothermia and severe epileptic seizures, highlighting combined contributions of different neuronal populations to the complex pathology in this model (Bolea et al., 2019). While the genetic defects underlying Leigh syndrome are well documented, the biochemical mechanisms linking the bioenergetic deficit to the onset of neurodegeneration remain ill defined. Some evidence for oxidative stress has been documented, (Lee et al., 2019; Song et al., 2017; de Haas et al., 2017,); but is more often described in total brain preparations or lesser-affected regions of the Ndufs4 KO brain. Other reports show no increase in protein carbonylation in the pathologically lesioned BS or OB (Kayser et al., 2016; Piroli et al., 2016, Johnson et al., 2020), and specific measurement of the rate of H_2O_2 production by mitochondria respiring on malate and pyruvate demonstrated no difference in the Ndufs4 KO versus WT (Jain et al., 2019).

In contrast, reductive stress is an established component of impaired OXPHOS during mitochondrial disease (Titov et al., 2016). We have shown that elevated $NADH/NAD^+$ is associated with tricarboxylic acid (TCA) cycle alterations to increase fumarate and protein succination in the affected Ndufs4 KO brain (Piroli et al. 2016). Succination is a covalent chemical modification of protein cysteine thiols following non-enzymatic modification by fumarate, generating S-2-succinocysteine (2SC) (Figure S1A, Alderson et al., 2006; Frizzell et al., 2009; Merkley et al., 2014), a modification that contributes to reduced protein function (Manuel et al., 2017; Piroli et al. 2014; Ternette et al. 2014). Thiol reactivity with protonated fumarate is enhanced in an acidic microenvironment (Kulkarni et al. 2019), driven by lactic acidosis in the Ndufs4 KO brain. We confirmed increased succination of select proteins in lesioned Ndufs4 KO brain regions such as the vestibular nucleus, including tubulin and mitochondrial voltage-dependent anion channels (VDAC) 1 and 2 (Piroli et al., 2016). In the current study, we demonstrate that mitochondrial dihydrolipoyllysine-residue succinyltransferase (DLST), a component of the α-ketoglutarate dehydrogenase complex (KGDHC), is uniquely succinated in the Ndufs4 KO brain. KGDHC is arguably the rate limiting step of the TCA cycle in the brain (Sheu and Blass, 1999), suggesting that impaired activity of this complex would have pronounced effects when OXPHOS is defective. We report the striking functional impact of DLST succination by fumarate on distinct mitochondrial metabolic processes; exacerbating mitochondrial ATP deficiency independent of the existing genetic Complex I bioenergetic defect.

Results

Dihydrolipoyllysine-residue succinyltransferase is succinated in the Ndufs4 KO mouse brain

We sought to identify a consistently succinated protein detected primarily in the brainstem (BS) and olfactory bulb (OB) of the Ndufs4 KO mouse. This immunoreactive band was located at ~48-50 kDa with anti-2SC antibody, which is immediately below the succinated tubulin band (Piroli et al., 2016). Using high speed centrifugation to remove abundant cytosolic tubulin, we confirmed that this succinated band was present in KO, but not in WT mice BS preparations (Figure 1A, arrow in 2SC panel), and was further enriched following depletion of tubulin (Figure S1B, arrow in 2SC panel). To characterize succinated proteins we isolated gliosomes and synaptosomes from WT and Ndufs4 KO mouse BS; this gradient preparation generates a loose pellet that was saved for comparative analysis. Glial fibrillary acidic protein (GFAP), an astrocytic marker, was enriched in the gliosomes, whereas the presence of the neuronal presynaptic marker synaptophysin was prominent in the synaptosomes (Figure 1B, GFAP and synaptophysin panels). The outer mitochondrial membrane marker VDAC2 was present in the homogenate and the synaptosomes, and further enriched in the pellet fractions (Figure 1B, VDAC2 panel). Overall, the pellets were rich in mitochondria but devoid of cytosolic, synaptic and astroglial markers. After probing with anti-2SC antibody, the succinated band at ~48-50 kDa was notably enriched in the pellet fraction of Ndufs4 KO but not in WT mice (Figure 1B, arrow in 2SC panel). Tubulin depletion facilitated this visualization in the pellets (Figure 1B, α-tubulin panel); as the abundant presence of succinated tubulin both in WT and KO preparations overwhelms the detection of this ~48-50 kDa band in other fractions (Figure 1B, 2SC panel). Similar results were obtained with preparations from the cerebellum (CB), another affected brain region in Ndufs4 KO mice (Figure S1C, D). To identify this succinated protein, the pellet fractions were further separated by SDS-PAGE, with parallel lanes used for anti-2SC immunoblotting or Coomassie staining, prior to band excision and LC-MS/MS mass spectrometry. This proteomic strategy identified the mitochondrial form of the dihydrolipoyllysine-residue succinyltransferase (DLST) component of the KGDHC, whose isoelectric point (pI) ~5.98 corresponded to a previously unidentified train of succinated spots on 2D-separated immunoblots (Piroli et al. 2016). The KGDHC comprises several copies of three subunits: α-ketoglutarate dehydrogenase (KGDH, E1k), DLST (E2k), and dihydrolipoamide dehydrogenase (DLD, E3) (Reed and Oliver, 1982), with E1k and E2k being specific for this complex and E3 shared with other α-ketoacid dehydrogenases (Reed, 1974). Supplemental Table 1 summarizes the DLST peptides confirmed by mass spectrometry, with the representative validated peptide NVETM^{OX}NYADIER ([M+2H]$^{2+}$: 735.8322, XCorr (+2) = 3.94) shown in Figure 1D. We analyzed total homogenates and purified mitochondrial fractions from WT and Ndufs4 KO mice to examine if the succinated protein paralleled DLST localization. Figure 1C shows that a low exposure of BS homogenates from KO and WT mice do not show detectable changes (2SC panel, homogenate lanes) due to the abundance of the succinated tubulin band (Piroli et al., 2014; Piroli et al., 2016). In contrast, mitochondrial purification allowed for resolution of the distinctly succinated ~48-50 kDa band in the KO (2SC panel, mitochondria lanes, black arrow). The additional succinated band at ~30-32 kDa had been previously identified as mitochondrial VDAC1 and 2 (Piroli et al., 2016). After stripping, a specific anti-DLST antibody showed similar levels of this protein in both WT and Ndufs4 KO mitochondria, with precise overlap with the succinated bands at ~48-50 kDa (DLST panel, 2SC panel, mitochondria lanes).

To specifically confirm if the DLST identification corresponded to the train of succinated spots previously observed on 2D immunoblots (Piroli et al. 2016), we performed 2D-gel electrophoresis of BS proteins to separate the tubulin isoforms from other proteins with similar MW but different pI. As shown in Figure 1D (2SC panels), succinated tubulins appeared as an intense spot at ~50-55 kDa that extends across the range of pI 4.7-5.4 both in WT and KO preparations, as previously reported (Piroli et al., 2014; Piroli et al., 2016). We focused our attention on the train of succinated spots at ~48-50 kDa (highlighted with a rectangle). In the KO preparation several spots were present in this area (Figure 1D, 2SC KO panel), whereas in the WT preparation only one spot was present (Figure 1D, 2SC WT panel). Using a DLST specific antibody a train of spots was detected both in the WT and KO blots (Figure 1D, DLST panels). In the WT blots, the four spots detected by anti-DLST do not overlap with any succinated spot (Figure 1D, WT DLST and 2SC panel). In contrast, three succinated spots co-localize with three of the spots in the DLST blot in KO preparations (Figure 1D, overlap marked by arrows in KO 2SC and DLST panels). Since the isoelectric focusing can contribute to uneven protein loading, we further confirmed that total DLST protein levels do not change in the BS between genotypes, as shown in Figure 1E and F. In summary, we confirmed that DLST is uniquely succinated by fumarate in the BS of Ndufs4 KO mice compared to WT mice.

Succination reduces the activity of the α-ketoglutarate dehydrogenase complex

We hypothesized that DLST succination driven by increased fumarate might affect the functionality of the KGDHC, since components of this complex are susceptible to oxidative modification (Chinopoulos et al., 1999; Humphries and Szweda, 1998; Starkov et al., 2004). We confirmed increased fumarate concentration in the OB of the Ndufs4 KO mouse (96.7% greater than in WT OB, $p<0.001$, Figure 2A), which accumulated in parallel with increased lactate (Figure 2B). Pyruvate and malate levels were also significantly increased in the Ndufs4KO (Figure S2). We then measured KGDHC activity in both the BS and OB of WT and Ndufs4 KO mice, and found that in both brain regions it was significantly lower in the KO mice (24.2 and 31.2% decrease in BS and OB, $p<0.05$ and 0.01 respectively, Figures 2C and 2D). Fumarate mediated reduction in the activity of the dehydrogenase was also confirmed *in vitro* following incubation of an isolated KGDHC standard with a range of dimethyl fumarate (DMF) concentrations, as treatment with this reactive fumarate ester also results in protein succination (Piroli et al., 2019). Figure 2E demonstrates that DMF treatment caused a dose-dependent decrease in the activity of the complex. Furthermore, we confirmed decreased KGDHC activity in N1E-115 neurons that were incubated with DMF for 18 h (Figure 2F). When we replaced DMF with dimethyl succinate, a DMF analog that does not modify cysteine residues due to the lack of the double bond, there was no loss of KGDHC activity (Figure 2F). Interestingly, increased succination of a band at ~48-50 kDa was observed in N1E-115 neurons after incubation with 50 and 100 µM DMF (Figure 2G, arrow in 2SC panel), and the band co-localized with DLST immunolabeling (Figure 2G, DLST panel). The specific reduction in KGDHC functionality following fumarate ester treatment supports the demonstration of reduced KGDHC activity in both the OB and BS, where endogenously produced fumarate and specific succination of DLST are elevated. Since the production of succinyl Co-A by KGDHC employs the formation of a DLST-mediated succinyl-dihydrolipoate intermediate; we investigated whether fumarate modification of the covalently associated lipoic acid decreased detection of lipoylated DLST in the KO (Figure S2E,F). Reduced detection of lipolylated DLST following a proposed oxidative modification has been documented (Bailey 2020), and we have previously shown that

fumarate modification of specific sites can decrease antibody recognition of other proteins (Piroli et al. 2014, 2019). We did not detect a reduction in the lipoylated DLST signal intensity (Figure S2E,F), therefore a cysteine, rather than the lipoic acid thiol, is the site of the fumarate adduct.

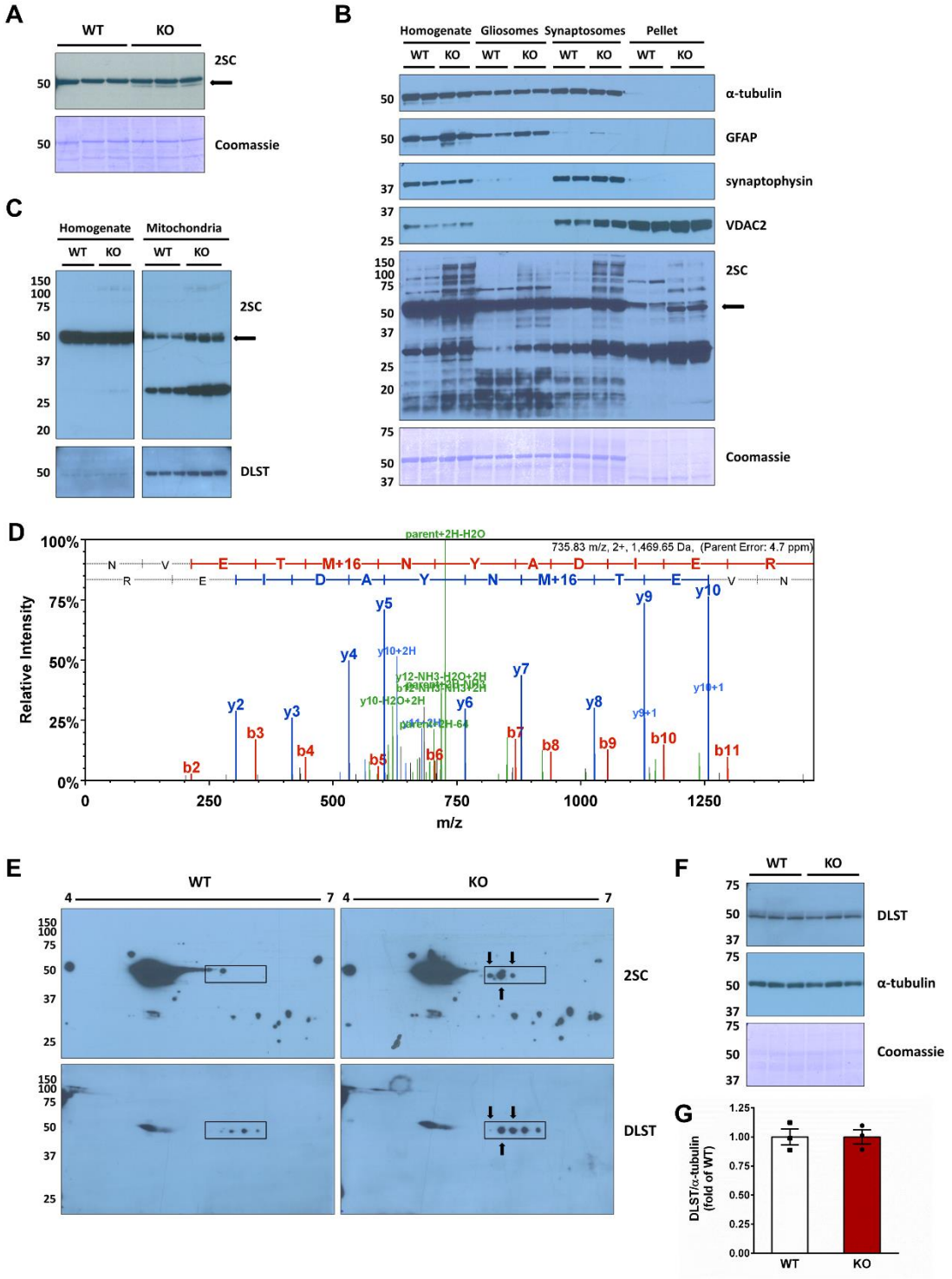

Figure 1: Identification of dihydrolipoyllysine-residue succinyltransferase (DLST) succination in the brainstem (BS) of the Ndufs4 KO mouse.

A, Detection of a distinct succinated band at ~48-50 kDa (arrow) in pellets obtained after high speed centrifugation of Ndufs4 KO BS homogenates. *B*, Characterization of the purity of homogenates, gliosomes, synaptosomes, and a pellet fraction obtained from BS by analysis of α-tubulin, GFAP, synaptophysin and VDAC2 expression. A ~48-50 kDa succinated band is present in the pellet fractions (2SC panel, KO lanes, arrow). *C*, Analysis of homogenates and purified mitochondrial preparations showing a succinated band at ~48-50 kDa in KO mitochondrial lanes (2SC panel, arrow), which overlapped with DLST detection. *D,* MS/MS spectrum of the peptide NVETM^{ox}NYADIER corresponding to DLST in a ~48-50 kDa band isolated from the pellet preparation used in *B*. *E*, Co-localization (arrows) of succinated spots with DLST-immunoreactive spots in the region of ~48-50 kDa and pH 5.5-6.3 (rectangular area) in Ndufs4 KO BS preparations. *F*, Total DLST and α-tubulin content in BS homogenates of WT and Ndufs4 KO mice. *G*, Quantification of the blots in *F*. See also Figure S1 and Table S1.

In *A*, *B*, *C*, *E* and *F*, molecular weight markers are shown on the left. Coomassie staining was used to verify even load of the lanes. In *G*, results expressed as means ± SEM were compared by unpaired t test (NS)

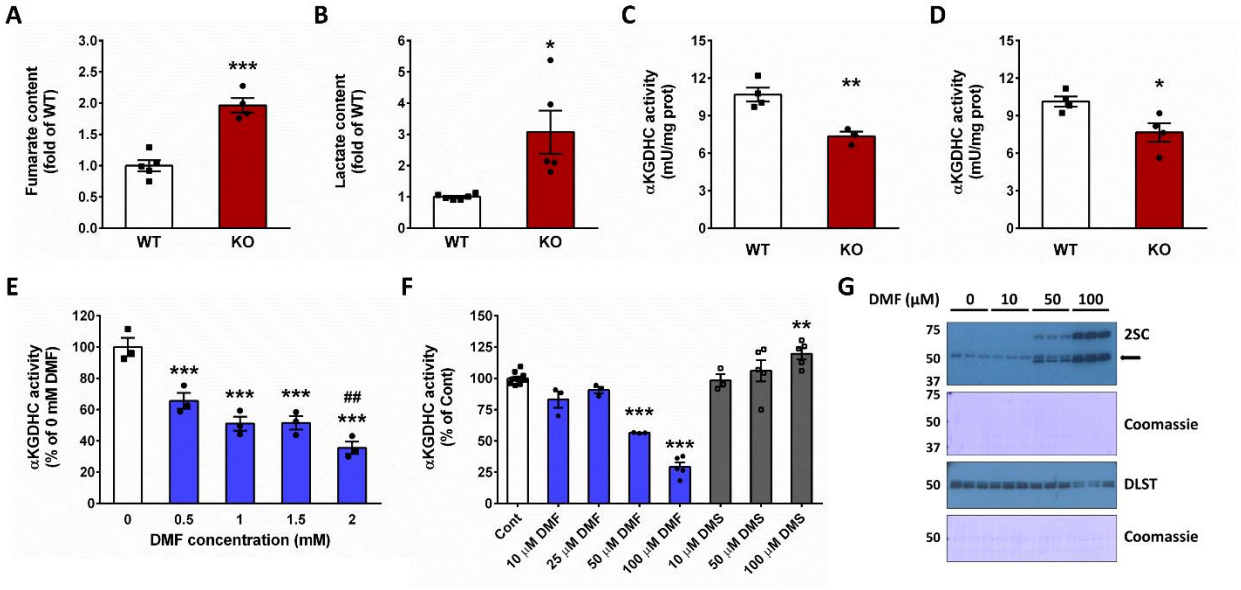

Figure 2: α-ketoglutarate dehydrogenase complex (KGDHC) activity is reduced as a consequence of fumarate derived protein succination.

A-B, Fumarate (*A*) and lactate (*B*) contents in the OB of Ndufs4 KO and WT mice. *C-D*, KGDHC activity in the BS (*C*) and OB (*D*) of Ndufs4 KO and WT mice. *E*, Effect of the incubation with dimethyl fumarate (DMF) on the activity of a bovine heart KGDHC standard. *F*, Effect of the addition of DMF or dimethyl succinate (DMS) to differentiated N1E-115 neurons on the KGDHC activity. *G*, Protein succination in N1E-115 neurons exposed to DMF. The succinated band at ~48-50 kDa (arrow) co-localized with DLST immunoreactivity. Molecular weight markers are shown on the left side. See also Figure S2.

Results are expressed as means ± SEM. In panels *A-D*, comparisons by unpaired t test; in panels *E-F*, comparisons by one-way ANOVA and *post hoc* Student-Neuman-Keuls test (* $p<0.05$, ** $p<0.01$ and ***$p<0.001$ vs. WT or untreated control; $^{\#\#}$ $p<0.01$ vs 0.5 mM DMF).

Substrate level phosphorylation is decreased in the Ndufs4 KO mouse brain.

Since decreased KGDHC activity would lead to reduced formation of succinyl CoA, this in turn would likely decrease the conversion of succinyl-CoA into succinate in the TCA cycle. This step is catalyzed by the enzyme succinyl-CoA ligase (SUCLA), which is responsible for the synthesis of GTP or ATP by substrate level phosphorylation (SLP). In rodents and human brain, succinyl-CoA ligase preferentially produces ATP, whereas in anabolic tissues the main product is GTP (Lambeth et al., 2004; Ostergaard, 2008). We measured total and SLP-linked ATP synthesis in mitochondria isolated from both OB and BS of WT and Ndufs4 KO mice. Under the conditions used, total ATP synthesis represents the sum of ATP production by OXPHOS and SLP, and the residual ATP synthesis in the presence of the ATP synthase inhibitor oligomycin represents SLP (Komlódi and Tretter, 2017). Using α-ketoglutarate as a substrate, total ATP synthesis was decreased by 42.5% ($p<0.05$), and SLP was decreased by 48.3% ($p<0.05$) in the OB of the KO mice (Figure 3A). These data demonstrate that, in addition to the Complex I defect in OXPHOS derived ATP production, the generation of TCA cycle derived intramitochondrial ATP is also compromised. In contrast, we observed no significant differences in total ATP synthesis and SLP in the BS of Ndufs4 KO vs. WT mice (Figure 3B). This may reflect the heterogeneity of the total BS mitochondrial preparation, where select nuclei are more affected by pathology. When succinate was used as a respiratory substrate, no differences in total ATP synthesis were observed for OB (Figure 3C) and BS (Figure 3D). As expected, succinate did not support SLP irrespective of the genotype and brain region (Figure 3C and D) (Komlódi and Tretter, 2017).

Succinylation of mitochondrial proteins is reduced in the Ndufs4 KO mouse brain

Decreased synthesis of succinyl-CoA could also be expected to reduce protein succinylation, a distinct acyl CoA derived modification (Zhang et al. 2011), in brain regions of the Ndufs4 KO mouse. Protein succinylation has been implicated in modulating the activity of mitochondrial enzymes (Gibson et al., 2015; Park et al., 2013). DLST can act as a protein succinyl transferase (Gibson et al., 2015), therefore the succination of DLST could contribute directly to decreased mitochondrial protein succinylation. As shown in Figure 4A, the intensity of lysine succinylation was markedly decreased in the mitochondrial fractions from BS of Ndufs4 KO mice compared to their WT littermates. The quantification of the signal reduction for the most intense bands demonstrated >50% reduction in the KO (Figure 4B). We also investigated total lysine succinylation levels in the nuclear fraction but found no change (Figure S3B). The expected reduction in succinyl-CoA levels is further represented by decreased levels of succinate in the OB of the Ndufs4 KO (Figure 4E). Given that metabolite flux through KGDHC is impaired, we predicted that acetyl CoA-derived mitochondrial lysine acetylation would be increased, this is shown for select proteins in the Ndufs4 KO versus the WT (Figures 4C & 4D, quantification for several acetylated protein bands was performed). Specific hyperacetylation of ATP synthase and pyruvate dehydrogenase (PDH) subunits, resulting in reduced PDH activity, has recently been described in specific glutamatergic Ndufs4 KO neurons (Gella et al. 2020). Figure 4F summarizes the impact of increased fumarate-mediated generation of 2-succocysteine (2SC) on DLST ($DLST^{2SC}$). Defective KGDHC activity results in lower ATP via reduced SUCLA activity, decreased lysine succinylation and increased lysine acetylation.

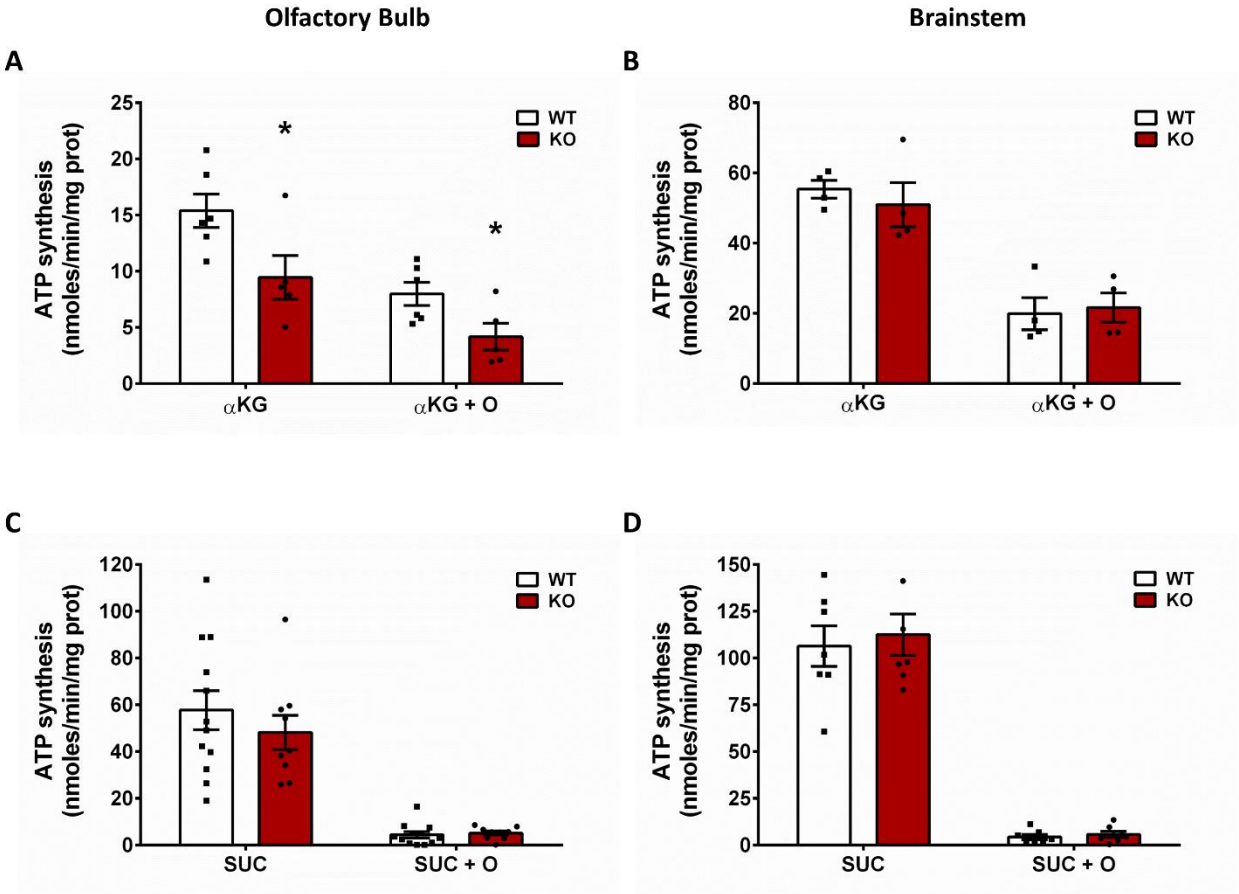

Figure 3*:* Total ATP synthesis and substrate level phosphorylation (SLP) are decreased in the olfactory bulb of the Ndufs4 KO mouse.

A-B, Total ATP synthesis (no oligomycin) and SLP (+8 µM oligomycin = O) in the olfactory bulb (OB, *A*) and the brainstem (BS, *B*) in the presence of 5 mM α-ketoglutarate (αKG) as respiratory substrate. *C-D*, Same as in *A-B* but using 5 mM succinate (SUC) as respiratory substrate.

Results are expressed as means ± SEM. Comparisons by unpaired t test (*$p<0.05$ vs. WT).

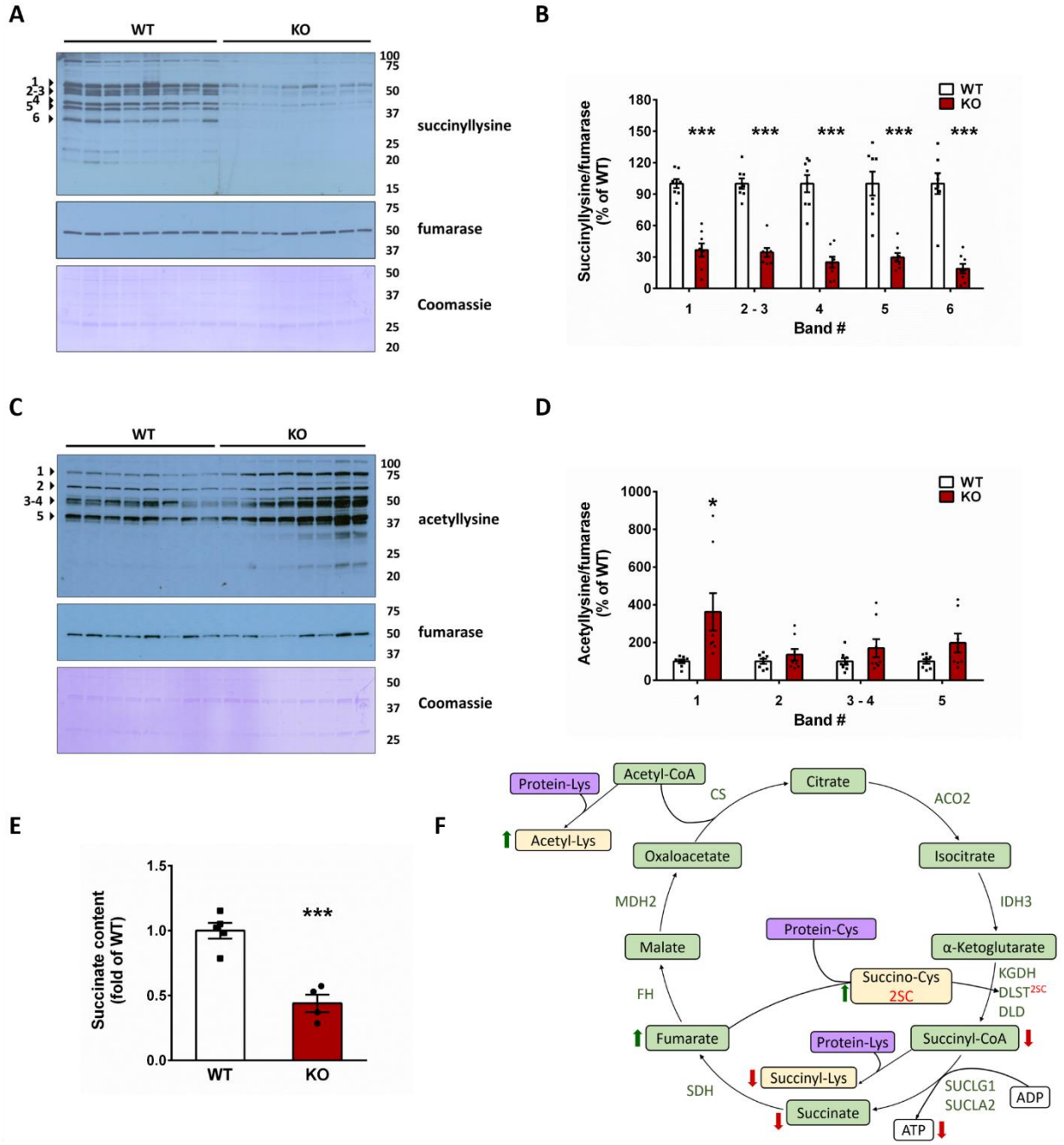

Figure 4: Succination of DLST alters the levels of protein acylation in the Ndufs4 KO brainstem

A, Protein lysine succinylation in mitochondrial fractions obtained from BS of WT and Ndufs4 KO mice. *B*, Quantification of prominent bands in *A* (arrowheads). *C*, Protein lysine acetylation in mitochondrial fractions obtained from BS of WT and Ndufs4 KO mice. *D*, Quantification of prominent bands in *C*

(arrowheads). *E*, Reduced production of succinate in OB of Ndufs4 KO vs. WT controls. F, Schematic summarizing the metabolic impact of increased fumarate production to increase production of succinated cysteines (2SC), with an emphasis on the direct effects of succinated DLST ($DLST^{2SC}$). Relationships between metabolites (green boxes), protein lysine or cysteine residues (purple boxes) and protein modifications (yellow boxes) are indicated.

In *A* and *C*, re-probing to detect fumarase for mitochondrial protein normalization, followed by Coomassie Brilliant Blue staining. Molecular weight markers are shown on the right side. See also Figure S3.

In *B*, *D* and *E* results expressed as means ± SEM were compared by unpaired t test (*$p<0.05$ and ***$p<0.001$ vs. WT).

Discussion

The results of the current study mechanistically demonstrate that DLST, a component of the KGDHC, is succinated by fumarate in the BS and OB of the Ndufs4 KO mouse, two brain regions with the most profound pathological changes in this model of Leigh syndrome (Quintana et al., 2010). Consistent with DLST succination, we quantified decreased activity of the KGDHC in these same brain regions of the Ndufs4 KO mouse. These important results link an OXPHOS genetic defect to impaired TCA function and defective succinyl-CoA production, a TCA intermediate necessary for SUCLA-mediated SLP (Kiss et al., 2013; Komlódi and Tretter, 2017) and succinylation reactions (see schematic in Figure 4F, Yang and Gibson, 2019). While variable redox changes modulate TCA cycle activity depending on the energy status of the cell, protein succination represents a static event that contributes to functional insufficiency of the affected proteins, elucidating an unrecognized pathological contributor in Complex I deficiency. The increase in fumarate levels despite significantly reduced KGDHC activity and succinate production reflect metabolic rewiring of the TCA cycle under conditions of reductive stress and lactic acidosis, where oxidative decarboxylation of malate by malate dehydrogenase (MDH2) is limited and malate and fumarate accumulate. In contrast, the oxidation of succinate is favored in the Ndufs4 KO to supply electrons for OXPHOS via $FADH_2$ generation.

The role of KGDHC deficiency in neurodegeneration has been extensively studied in the preclinical setting, including the genetic modulation of DLD and DLST; in both cases the KO mice were not viable (Johnson et al., 1997; Yang et al., 2009). $DLST^{+/-}$ and $DLD^{+/-}$ do not show overt symptoms but are susceptible to mitochondrial toxins used to replicate neurodegenerative diseases (Klivenyi et al., 2004; Yang et al., 2009). Pharmacological inhibition of KGDHC activity *in vitro* alters mitochondrial morphology and increases fission and mitophagy (Banerjee et al., 2016). Human patients with mutations in the *LIPT1/2* genes that encode a lipoyltransferase necessary for DLST lipoylation develop Leigh Syndrome-like encephalopathies (Habarou et al., 2017; Stowe et al., 2018), supporting a role for defective KGDHC components in neuropathology. Of note, the expression of DLST in the human brain appears to be restricted exclusively to neurons (Dobolyi et al. 2020). Brain regions from patients with Alzheimer's disease (AD) show ~57% reduced KGDHC activity (Butterworth and Besnard, 1990; Gibson et al., 1988). Our studies elucidate that mitochondrial stress contributes to fumarate-driven reductions in KGDHC activity; the chemical modification of DLST by fumarate is therefore a novel determinant of KGDHC activity in the Ndufs4 KO model of Leigh syndrome. Interestingly, the degree of KGDHC inhibition in the brains of Ndufs4 KO mice is aligned with that reported using pharmacological inhibitors of the complex to impair mitochondrial function (Banerjee et al., 2016).

Previous reports on ATP synthesis levels in the Ndufs4 KO mouse vary depending on the tissue analyzed, with no differences in total cellular ATP content in immortalized fibroblasts (Valsecchi et al., 2012) and skeletal muscle (Alam et al., 2015; Kruse et al., 2008; Terburgh et al., 2019). However, neither fibroblasts not skeletal muscle show overt pathology, nor did we find evidence of increased succination in the skeletal muscle of the Ndufs4 KO compared to WT mice (Piroli et al. 2016). Maximal mitochondrial ATP production in the whole brain is slightly decreased in Ndufs4 KO *versus* WT mice (Manjeri et al., 2016), and CI-linked ATP synthesis was also slightly decreased in isolated permeabilized neurons and astrocytes from mice with a spontaneous mutation leading to disruption of *NDUFS4* (Bird et al., 2014). We report that both total and SLP-linked ATP synthesis in mitochondria isolated from the OB of the Ndufs4 KO mouse were

decreased when α-ketoglutarate, a preferential substrate for SLP, was used. A previous study using brain mitochondria from $DLD^{+/-}$ and $DLST^{+/-}$ mice showed diminished mitochondrial ATP efflux with fuel combinations that support SLP compared to WT mitochondria, and these mice also had a 20-48% decrease in KGDHC activity, which is consistent with our findings (Kiss et al., 2013). Our data provides novel mechanistic insight on the metabolic complexity of CI deficiency, elucidating how the mitochondria suffer from not only defective OXPHOS; but also have inadequate compensatory ATP generation via SLP. Reduced ATP production in the most susceptible neurons would accelerate their functional decline.

Since succinyl-CoA is also required for protein succinylation (Zhang et al., 2011), we predicted a decrease in this post-translational modification in the brain of the Ndufs4 KO mouse. We demonstrate a profound decrease in global mitochondrial succinylation. Alterations in succinylation had not been documented in mitochondrial encephalomyopathies until a recent report demonstrating hypersuccinylation in *SUCLA2* deficiency, a mtDNA depletion syndrome (Gut et al. 2020). Hypersuccinylation contrasts with the deficient succinylation that we report, but these striking differences may underlie the heterogeneity of the molecular and clinical phenotype of these Leigh-like encephalopathies. While the *SUCLA2* insufficiency has some clinical similarity with *NDUFS4* deficiency, other features such as sensorineural deafness and mtDNA depletion differ from the CI defect. Future studies will be required to decipher the role of metabolite-derived chemical modifications to drive these and other phenotypic differences. In contrast to cysteine succination, succinylation is reversible by specific sirtuin (SIRT) enzymes (Yang and Gibson, 2019). Overexpression of *SIRT5* increased survival and improved mitochondrial oxygen consumption in a zebrafish model of *SUCLA2* deficiency, but did not increase mtDNA content, suggesting that hypersuccinylation in the presence of elevated succinyl CoA contributes to defined phenotypic outcomes (Gut et al. 2020). KGDHC can succinylate proteins *in vitro* more efficiently than free succinyl-CoA, likely due to the succinyl-transferase activity of the E2 component (Gibson et al., 2015). In agreement with our observations in the Ndufs4 KO, KGDHC inhibitors reduce succinylation of cytosolic and mitochondrial proteins in primary neurons (Gibson et al., 2015). Targeted studies on the impact of protein hypo/hyper-succinylation in genetic mitochondrial diseases should further elucidate additional mechanisms governing cellular decline.

Hypoxia has been shown to prolong lifespan and reduce brain lesions in the Ndufs4 KO mouse (Jain et al., 2016; Ferrari et al., 2017). Reduction in the oxygen content in the air normalizes the hyperoxia present in the brain of the Ndufs4 KO mouse to levels found in WT littermates breathing normal air (Jain et al., 2019). Interestingly, *in vitro* studies with N2a neural cells showed that hypoxia leads to increased mitochondrial protein succinylation (Chen et al., 2017), therefore it will be of interest to determine if hypoxia treatment can alleviate the decreased lysine succinylation observed in the Ndufs4 KO mouse. In addition, dimethyl α-ketoglutarate (DMKG), a cell permeable form of α-ketoglutarate, has been shown to delay neurological symptoms and increase the median lifespan of Ndufs4 KO by ~40 days (Lee et al., 2019). While DMKG supplementation will augment succinyl CoA and confer benefit by providing electrons to support Complex-II dependent respiration; it still does not bypass the defective KGDHC activity caused by the succination of DLST. Future targeted studies to reduce fumarate accumulation are expected prevent the sustained damage caused by covalent protein succination during reductive stress, and improve the response to supplementary therapies, such as DMKG, to benefit neuronal survival during Leigh Syndrome.

Significance

The biochemical mechanisms driving neuropathology in mitochondrial oxidative phosphorylation (OXPHOD) disorders, such as Leigh syndrome, are not well understood beyond the known ATP deficit. Therapeutic approaches to treat the mitochondrial diseases employ vitamins and antioxidants, yet there is limited evidence for oxidative stress as a driver of neurological decline. In contrast, reductive stress is associated with lactic acidosis and altered tricarboxylic acid (TCA) cycle metabolism. We demonstrate that fumarate levels are increased in brain regions of the *NDUFS4* knockout mouse model of mitochondrial Complex I deficiency. Increased fumarate reacts covalently with protein thiols to generate the chemical modification 2-succinocysteine (protein succination). We report that the specific succination of dihydrolipoyllysine-residue succinyltransferase (DLST) irreversibly reduces the activity of the α-ketoglutarate dehydrogenase complex (KGDHC). This persistent deficit worsens the mitochondrial OXPHOS derived ATP deficit by limiting compensatory substrate level phosphorylation (SLP) via succinyl CoA ligase. Defective KGDHC activity also reduces succinyl CoA mediated lysine succinylation, a distinct acyl modification, in the affected brain regions of the Ndufs4 knockout mouse. The data mechanistically demonstrates how altered TCA cycle metabolism drives the chemical modification of proteins to disrupt metabolic homeostasis; and provides a novel biochemical basis for mitochondrial pathophysiology during Complex I OXPHOS deficiency.

Author Contributions

G.G.P and N.F. designed the research. G.G.P., R.S.M., A.M.M., H.H.S., W.E.C, and M.D.W. performed experiments. G.G.P., R.S.M., A.M.M., H.H.S., W.E.C, M.D.W. and N.F. analyzed data. G.G.P., A.M.M., and N.F. wrote the paper.

Acknowledgements

This work was supported by the National Institutes of Health (R56 NS116174, R01 NS092938, R03 HD077187, F31 DK108559), National Science Foundation (1828059), and a University of South Carolina Research Foundation ASPIRE-I award.

References

Alam, M.T., Manjeri, G.R., Rodenburg, R.J., Smeitink, J.A., Notebaart, R.A., Huynen, M., Willems, P.H., and Koopman, W.J. (2015). Skeletal muscle mitochondria of NDUFS4-/- mice display normal maximal pyruvate oxidation and ATP production. Biochim. Biophys. Acta *1847*, 526-533.

Alderson, N.L., Wang, Y., Blatnik, M., Frizzell, N., Walla, M.D., Lyons, T.J., Alt, N., Carson, J.A., Nagai, R., Thorpe, S.R., et al. (2006). S-(2-Succinyl)cysteine: A novel chemical modification of tissue proteins by a Krebs cycle intermediate. Arch. Biochem. Biophys. *450*, 1-8.

Bailey, P.S.J., Ortmann, B.M., Martinelli, A.W., Houghton, J.W., Costa, A.S.H., Burr, S.P., Antrobus, R., Frezza, C., and Nathan, J.A. (2020) ABHD11 maintains 2-oxoglutarate metabolism by preserving functional lipoylation of the 2-oxoglutarate dehydrogenase complex. Nat. Commun. 11:4046. doi: 10.1038/s41467-020-17862-6.

Banerjee, K., Munshi, S., Xu, H., Frank, D.E., Chen, H.L., Chu, C.T., Yang, J., Cho, S., Kagan, V.E., Denton, T.T., et al. (2016). Mild mitochondrial metabolic deficits by α-ketoglutarate dehydrogenase inhibition cause prominent changes in intracellular autophagic signaling: Potential role in the pathobiology of Alzheimer's disease. Neurochem. Int. *96*, 32-45.

Bird, M.J., Wijeyeratne, X.W., Komen, J.C., Laskowski, A., Ryan, M.T., Thorburn, D.R., and Frazier, A.E. (2014). Neuronal and astrocyte dysfunction diverges from embryonic fibroblasts in the Ndufs4fky/fky mouse. Biosci. Rep. *34*:e00151.

Bolea, I., Gella, A., Sanz, E., Prada-Dacasa, P., Menardy, F., Bard, A.M., Machuca-Márquez, P., Eraso-Pichot, A., Mòdol-Caballero, G., Navarro, X., et al. (2019). Defined neuronal populations drive fatal phenotype in a mouse model of Leigh syndrome. eLife *8*:e47163.

Butterworth, R.F., and Besnard, A.M. (1990). Thiamine-dependent enzyme changes in temporal cortex of patients with Alzheimer’s disease. Metab. Brain. Dis. *5*, 179-184.

Calvaruso, M.A., Willems, P., van den Brand, M., Valsecchi, F., Kruse, S., Palmiter, R., Smeitink, J., and Nijtmans, L. (2011). Mitochondrial complex III stabilizes complex I in the absence of NDUFS4 to provide partial activity. Hum. Mol. Genet. *21*:115-120.

Carney, K.E., Milanese, M., van Nierop, P., Li, K.W., Oliet, S.H., Smit, A.B., Bonanno, G., and Verheijen, M.H. (2014). Proteomic analysis of gliosomes from mouse brain: identification and investigation of glial membrane proteins. J. Proteome Res. *13*, 5918–5927.

Chen, H., Xu, H., Potash, S., Starkov, A., Belousov, V.V., Bilan, D.S., Denton, T.T., and Gibson, G.E. (2017). Mild metabolic perturbations alter succinylation of mitochondrial proteins. J. Neurosci. Res. *95*, 2244-2252.

Chinopoulos, C., Tretter, L., and Adam-Vizi, V. (1999). Depolarization of in situ mitochondria due to hydrogen peroxide-induced oxidative stress in nerve terminals: inhibition of alpha-ketoglutarate dehydrogenase. J Neurochem. *73*, 220–228.

de Haas, R., Das, D., Garanto, A., Renkema, H.G., Greupink, R., van den Broek, P., Pertijs, J., Collin, R.W.J., Willems, P., Beyrath, J.,et al. (2017). Therapeutic effects of the mitochondrial ROS-redox modulator KH176 in a mammalian model of Leigh Disease. Sci. Rep. *7*:11733.

Dobolyi, A., Bago, A., Palkovits, M., Nemeria, N.S., Jordan, F., Doczi, J., Ambrus, A., Adam-Vizi, V., Chinopoulos, C. (2020) Exclusive neuronal detection of KGDHC-specific subunits in the adult human brain cortex despite pancellular protein lysine succinylation. Brain Struct. Funct. *225,* 639-667.

Ferrari, M., Jain, I.H., Goldberger, O., Rezoagli, E., Thoonen, R., Cheng, K.H., Sosnovik, D.E., Scherrer-Crosbie, M., Mootha, V.K., and Zapol, W.M. (2017). Hypoxia treatment reverses neurodegenerative disease in a mouse model of Leigh syndrome. Proc. Natl. Acad. Sci. U S A. *114*, E4241-E4250.

Frizzell, N., Rajesh, M., Jepson, M.J., Nagai, R., Carson, J.A., Thorpe, S.R., and Baynes, J.W. (2009). Succination of thiol groups in adipose tissue proteins in diabetes: Succination inhibits polymerization and secretion of adiponectin. J. Biol. Chem. *284*, 25772-25781.

Gella, A., Prada-Dacasa, P., Carrascal, M., Urpi, A., González-Torres, M., Abian, J., Sanz, E., and Quintana, A. (2020) Mitochondrial proteome of affected glutamatergic neurons in a mouse model of Leigh syndrome. Front. Cell. Dev. Biol. *8,* 660.

Gibson, G.E., Sheu, K.F.R., Blass, J.P., Baker, A., Carlson, K.C., Harding, B., and Perrino, P. (1988). Reduced activities of thiamine-dependent enzymes in the brains and peripheral tissues of patients with Alzheimer's disease. Arch. Neurol. *45*, 836–840.

Gibson, G.E., Xu, H., Chen, H.L., Chen, W., Denton, T.T., and Zhang, S. (2015). Alpha-ketoglutarate dehydrogenase complex-dependent succinylation of proteins in neurons and neuronal cell lines. J. Neurochem. *134*, 86-96.

Gut, P., Matilainen, S., Meyer, J.G., Pällijeff, P., Richard, J., Carroll, C.J., Euro, L., Jackson, C.B., Isohanni, P., Minassian, B.A., et al. (2020) SUCLA2 mutations cause global protein succinylation contributing to the pathomechanism of a hereditary mitochondrial disease. Nat. Commun. 11, 5927. doi: 10.1038/s41467-020-19743-4.

Habarou, F., Hamel, Y., Haack, T.B., Feichtinger, R.G., Lebigot, E., Marquardt, I., Busiah, K., Laroche, C., Madrange, M., Grisel, C., et al. (2017). Biallelic mutations in LIPT2 cause a mitochondrial lipoylation defect associated with severe neonatal encephalopathy. Am. J. Hum. Genet. *101*, 283-290.

Humphries, K.M., and Szweda, L.I. (1998). Selective inactivation of α-ketoglutarate dehydrogenase and pyruvate dehydrogenase: Reaction of lipoic acid with 4-hydroxy-2-nonenal. Biochemistry *37*, 15835-15841.

Jain, I.H., Zazzeron, L., Goldberger, O., Marutani, E., Wojtkiewicz, G.R., Ast, T., Wang, H., Schleifer, G., Stepanova, A., Brepoels, K., et al. (2019). Leigh Syndrome mouse model can be rescued by interventions that normalize brain hyperoxia, but not HIF activation. Cell Metab. *30*, 824-832.

Jain, I.H., Zazzeron, L., Goli, R., Alexa, K., Schatzman-Bone, S., Dhillon, H., Goldberger, O., Peng, J., Shalem, O., Sanjana, N.E., et al. (2016). Hypoxia as a therapy for mitochondrial disease. Science *352*, 54-61.

Johnson, M.T., Yang, H.S., Magnuson, T., and Patel, M.S. (1997). Targeted disruption of the murine dihydrolipoamide dehydrogenase gene (Dld) results in perigastrulation lethality. Proc. Natl. Acad. Sci. U S A. *94*, 14512-14517.

Johnson, S.C., Kayser, E.B., Bornstein, R., Stokes, J., Bitto, A., Park, K.Y., Pan, A., Sun, G., Raftery, D., Kaeberlein, M., Sedensky, M.M., and Morgan, P.G. (2020) Regional metabolic signatures in the Ndufs4(KO) mouse brain implicate defective glutamate/α-ketoglutarate metabolism in mitochondrial disease. Mol. Genet. Metab. *130,* 118-132.

Kayser, E.B., Sedensky, M.M., and Morgan, P.G. (2016). Region-specific defects of respiratory capacities in the Ndufs4(KO) mouse brain. PLoS One *11*:e0148219.

Kiss, G., Konrad, C., Doczi, J., Starkov, A.A., Kawamata, H., Manfredi, G., Zhang, S.F., Gibson, G.E., Beal, M.F., Adam-Vizi, V., et al. (2013). The negative impact of α-ketoglutarate dehydrogenase complex deficiency on matrix substrate-level phosphorylation. FASEB J. *27*, 2392-2406.

Klivenyi, P., Starkov, A.A., Calingasan, N.Y., Gardian, G., Browne, S.E., Yang, L., Bubber, P., Gibson, G.E., Patel, M.S., and Beal, M.F. (2004). Mice deficient in dihydrolipoamide dehydrogenase show increased vulnerability to MPTP, malonate and 3-nitropropionic acid neurotoxicity. J. Neurochem. *88*, 1352-1360.

Komlódi, T., and Tretter, L. (2017). Methylene blue stimulates substrate-level phosphorylation catalyzed by succinyl-CoA ligase in the citric acid cycle. Neuropharmacology *123*, 287-298.

Kruse, S.E., Watt, W.C., Marcinek, D.J., Kapur, R.P., Schenkman, K.A., and Palmiter, R.D. (2008). Mice with mitochondrial complex I deficiency develop a fatal encephalomyopathy. Cell Metab. *7*, 312–320.

Kulkarni, R.A., Bak, D.W., Wei, D., Bergholtz, S.E., Briney, C.A., Shrimp, J.H., Alpsoy, A., Thorpe, A.L., Bavari, A.E., Crooks, D.R., et al. (2019). A chemoproteomic portrait of the oncometabolite fumarate. Nat. Chem. Biol. *15*, 391-400.

Lake, N.J., Compton, A.G., Rahman, S., and Thorburn, D.R. (2016). Leigh syndrome: One disorder, more than 75 monogenic causes. Ann. Neurol. *79*, 190–203.

Lambeth, D.O., Tews, K.N., Adkins, S., Frohlich, D., and Milavetz, B.I. (2004). Expression of two succinyl-CoA synthetases with different nucleotide specificities in mammalian tissues. J. Biol. Chem. 279, 36621-36624.

Lee, C.F., Caudal, A., Abell, L., Nagana Gowda, G.A., and Tian, R. (2019). Targeting NAD^+ metabolism as interventions for mitochondrial disease. Sci. Rep. *9*:3073.

Lowry, O. H., Rosenbrough, N. J., Farr, A. L. and Randall, R. J. (1951). Protein measurement with the Folin phenol reagent. J. Biol. Chem. *193*, 265–275.

Manjeri, G.R., Rodenburg, R.J., Blanchet, L., Roelofs, S., Nijtmans, L.G., Smeitink, J.A., Driessen, J.J., Koopman, W.J., and Willems, P.H. (2016). Increased mitochondrial ATP production capacity in brain of healthy mice and a mouse model of isolated complex I deficiency after isoflurane anesthesia. J. Inherit. Metab. Dis. *39*, 59-65.

Manuel, A.M., Walla, M.D., Faccenda, A., Martin, S.L., Tanis, R.M., Piroli, G.G., Adam, J., Kantor, B., Mutus, B., Townsend, D.M., et al. (2017). Succination of protein disulfide isomerase links mitochondrial stress and endoplasmic reticulum stress in the adipocyte during diabetes. Antioxid. Redox Signal. *27*, 1281-1296.

Manuel, A.M., Walla, M.D., Dorn, M.T., Tanis, R.M., Piroli, G.G., and Frizzell N. (2020) Fumarate and oxidative stress synergize to promote stability of C/EBP homologous protein in the adipocyte. Free Radic. Biol. Med. *14,* 70-82.

Merkley, E.D., Metz, T.O., Smith, R.D., Baynes, J.W., and Frizzell, N. (2014). The succinated proteome. Mass Spectrom. Rev. *33*, 98-109.

Nagai, R., Brock, J. W., Blatnik, M., Baatz, J. E., Bethard, J., Walla, M. D., Thorpe, S. R., Baynes, J. W., and Frizzell, N. (2007). Succination of protein thiols during adipocyte maturation: a biomarker of mitochondrial stress. J. Biol. Chem. *282*, 34219–34228.

Oldham, W.M., and Loscalzo, J. (2016) Quantification of 2-Hydroxyglutarate Enantiomers by Liquid Chromatography-mass Spectrometry. Bio. Protoc. 6:e1908. doi: 10.21769/BioProtoc.1908.

Ortigoza-Escobar, J.D., Oyarzabal, A., Montero, R., Artuch, R., Jou, C., Jiménez, C., Gort, L., Briones, P., Muchart, J., López-Gallardo, E., et al. (2016). Ndufs4 related Leigh syndrome: A case report and review of the literature. Mitochondrion *28*, 73-78.

Park, J., Chen, Y., Tishkoff, D.X., Peng, C., Tan, M., Dai, L., Xie, Z., Zhang, Y., Zwaans, B.M.M., Skinner, M.E., Lombard, D.B., and Zhao, Y. (2013). SIRT5-mediated lysine desuccinylation impacts diverse metabolic pathways. Mol. Cell *50*, 919–930.

Piroli, G.G., Jepson, M.J., Manuel, A.M., Walla, M.D., Brock, J.W.C., Rajesh, M.P., Tanis, R.M., Cotham, W.E., and Frizzell, N. (2014). Identification of protein succination as a novel modification of tubulin. Biochem. J. *462*, 231-245.

Piroli, G.G., Manuel, A.M., Clapper, A.C., Walla, M.D., Baatz, J.E., Palmiter, R.D., Quintana, A., and Frizzell, N. (2016). Succination is increased on select proteins in the brainstem of the NADH dehydrogenase (ubiquinone) Fe-S protein 4 (Ndufs4) knockout mouse, a model of Leigh Syndrome. Mol. Cell. Proteomics *15*, 445-461.

Piroli, G.G., Manuel, A.M., Patel, T., Walla, M.D., Shi, L., Lanci, S.A., Wang, J., Galloway, A., Ortinski, P.I., Smith, D.S., et al. (2019). Identification of novel protein targets of dimethyl fumarate modification in

neurons and astrocytes reveals actions independent of Nrf2 stabilization. Mol. Cell. Proteomics *18*, 504-519.

Quintana, A., Kruse, S.E., Kapur, R.P., Sanz, E., and Palmiter, R.D. (2010). Complex I deficiency due to loss of Ndufs4 in the brain results in progressive encephalopathy resembling Leigh syndrome. Proc. Natl. Acad. Sci. U S A. *107*, 10996-11001.

Reed, L.J. (1974). Multienzyme complexes. Acc. Chem. Res. *7*, 40-46.

Reed, L.J., and Oliver, R.M. (1982). Structure-function relationships in pyruvate and α-ketoglutarate dehydrogenase complexes. Adv. Exp. Med. Biol. *148*, 231-241.

Schneider, C.A., Rasband, W.S., and Eliceiri, K.W. (2012). NIH Image to ImageJ: 25 years of image analysis. Nat. Methods *9*, 671–675.

Sheu, K.F.R., and Blass, J.P. (1999). The α-ketoglutarate dehydrogenase complex. Ann. N Y Acad. Sci. *893*, 61-78.

Song, L., Yu, A., Murray, K., and Cortopassi, G. (2017). Bipolar cell reduction precedes retinal ganglion neuron loss in a complex 1 knockout mouse model. Brain Res. *1657*, 232-244.

Starkov, A.A., Fiskum, G., Chinopoulos, C., Lorenzo, B.J., Browne, S.E., Patel, M.S., Beal, M.F. (2004) Mitochondrial alpha-ketoglutarate dehydrogenase complex generates reactive oxygen species. J. Neurosci. *24*, 7779–7788.

Stowe, R.C., Sun, Q., Elsea, S.H., and Scaglia, F. (2018). LIPT1 deficiency presenting as early infantile epileptic encephalopathy, Leigh disease, and secondary pyruvate dehydrogenase complex deficiency. Am. J. Med. Genet. A. *176*, 1184-1189.

Tanis, R.M., Piroli, G.G., Day, S.D., and Frizzell, N. (2015). The effect of glucose concentration and sodium phenylbutyrate treatment on mitochondrial bioenergetics and ER stress in 3T3-L1 adipocytes. Biochim. Biophys. Acta *1853*, 213-221.

Terburgh, K., Lindeque, Z., Mason, S., van der Westhuizen, F., and Louw, R. (2019). Metabolomics of Ndufs4$^{-/-}$ skeletal muscle: Adaptive mechanisms converge at the ubiquinone-cycle. Biochim. Biophys. Acta Mol. Basis Dis. *1865*, 98-106.

Ternette, N., Yang, M., Laroyia, M., Kitagawa, M., O'Flaherty, L., Wolhulter, K., Igarashi, K., Saito, K., Kato, K., Fischer, R., et al. (2013). Inhibition of mitochondrial aconitase by succination in fumarate hydratase deficiency. Cell Rep. *3*, 689-700.

Titov, D.V., Cracan, V., Goodman, R.P., Peng, J., Grabarek, Z., and Mootha, V.K. (2016). Complementation of mitochondrial electron transport chain by manipulation of the NAD^+/NADH ratio. Science. *352*, 231-235.

Yang, Y., and Gibson, G.E. (2019). Succinylation links metabolism to protein functions. Neurochem. Res. *44*, 2346-2359.

Yang, L., Shi, Q., Ho, D.J., Starkov, A.A., Wille, E.J., Xu, H., Chen, H.L., Zhang, S., Stack, C.M., Calingasan, N.Y., et al. (2009). Mice deficient in dihydrolipoyl succinyl transferase show increased vulnerability to mitochondrial toxins. Neurobiol. Dis. *36*, 320–330.

Zhang, Z., Tan, M., Xie, Z., Dai, L., Chen, Y., and Zhao, Y. (2011). Identification of lysine succinylation as a new post-translational modification. Nat. Chem. Biol. *7*, 58-63.

STAR Methods

KEY RESOURCES TABLE

REAGENT or RESOURCE	SOURCE	IDENTIFIER
Antibodies		
Acetylated-lysine rabbit Ab	Cell Signaling Technology	Cat # 9441 RRID:AB_331805
DLST rabbit Ab	Bethyl Laboratories	Cat # A304-309A-T RRID:AB_2781818
Fumarase rabbit mAb	Cell Signaling Technology	Cat#4567 RRID:AB_11178522
GFAP mouse mAb	Cell Signaling Technology	Cat#3670 RRID:AB_561049
Lipoic acid rabbit Ab	Millipore	Cat#437695 RRID:AB_212120
Pan succinyllysine rabbit Ab	PTM BIO	Cat#PTM-401 RRID:AB_2687628
Synaptophysin mouse mAb	Cell Signaling Technology	Cat#12270 RRID:AB_2797864
α-tubulin mouse mAb antibody	Cell Signaling Technology	Cat#3873 RRID:AB_1904178
βIII-tubulin rabbit mAb	Cell Signaling Technology	Cat#5666 RRID:AB_10691594
VDAC2 rabbit Ab	GeneTex	Cat#GTX104745 AB_1241440
2SC rabbit Ab	Nagai et al., 2007	Custom made
Bacterial and Virus Strains		
Biological Samples		
Chemicals, Peptides, and Recombinant Proteins		
Acetonitrile	Fisher Scientific	Cat#AC610010040
Acetic acid	Sigma-Aldrich	Cat#695092
Adenosine 5’-diphosphate	Sigma-Aldrich	Cat#A2754
Adenosine 5’-triphosphate	Sigma-Aldrich	Cat#A2383
Ammonium bicarbonate	Sigma-Aldrich	Cat#09830
Ammonium hydroxide	Fisher Scientific	Cat#A669-212
Bovine Serum Albumin	Sigma-Aldrich	Cat#A8806
Calcium chloride	Sigma-Aldrich	Cat#C3881
Coenzyme A	Sigma-Aldrich	Cat#C3144
Coomassie Brilliant Blue	Sigma-Aldrich	Cat#B7920
Criterion polyacrylamide gels	Bio-Rad Laboratories	Cat#567-1043
Diacetyl-L-tartaric anhydride	Sigma-Aldrich	Cat#358924
P^1,P^5-Di(adenosine-5’) pentaphosphate, trilithium salt	Sigma-Aldrich	Cat#D6392
Dimethyl fumarate	Sigma-Aldrich	Cat#242926

Dimethyl succinate	Sigma-Aldrich	Cat#73605
Dimethyl sulfoxide	Alfa Aesar	Cat#32434
Dithiothreitol	Sigma-Aldrich	Cat#D0632
DMEM	Thermo Fisher Scientific	Cat#12430-054
DPBS	Corning Cellgro	Cat#21-030-CV
EDTA	Sigma-Aldrich	Cat#ED2SS
EGTA	Sigma-Aldrich	Cat#324626
Ethyl acetate	Sigma-Aldrich	Cat#270989
Fetal bovine serum	Atlanta Biologicals	Cat#S11150
Formic acid	Sigma-Aldrich	Cat#100264
D-Glucose	Sigma-Aldrich	Cat#G8270
L-Glutamic acid, monosodium	Sigma-Aldrich	Cat#49621
Guanosine 5'-triphosphate	Cytoskeleton	Cat#BST06
HEPES	Sigma-Aldrich	Cat#H0527
Hexokinase/Glucose 6-phosphate dehydrogenase	Sigma-Aldrich	Cat#H8629
HyBlot CL Film	Thomas Scientific	Cat#1159M39
Hydrochloric acid	Sigma-Aldrich	Cat#258148
α-Ketoglutaric acid, disodium	Sigma-Aldrich	Cat#75892
α-Ketoglutarate dehydrogenase	Sigma-Aldrich	Cat#K1502
DL-lactic acid	Sigma-Aldrich	Cat#69785
L-lactic acid-$^{13}C_3$, sodium salt	Cambridge Isotope Laboratories	Cat#CLM1579
Magnesium chloride	Sigma-Aldrich	Cat#M1028
D-Mannitol	Sigma-Aldrich	Cat#M4125
2-Mercaptoethanol	Sigma-Aldrich	Cat#M6250
MES hydrate	Sigma-Aldrich	Cat#69890
Methanol	Fisher Scientific	Cat#A412-500
Methylamine	Sigma-Aldrich	Cat#395048
N-methyl-*N*-(trimethylsilyl) trifluoroacetamide	Sigma-Aldrich	Cat#69479
NAD^+	Sigma-Aldrich	Cat#N0632
$NADP^+$	Sigma-Aldrich	Cat#10128031001
Oligomycin	Sigma-Aldrich	Cat#O4876
Percoll	GE Healthcare	Cat#17-0891-02
Potassium chloride	Fisher Scientific	Cat#P217-500
Potassium phosphate, dibasic	Fisher Scientific	Cat#BP-363-500
Precision Plus protein ladder	BioRad Laboratories	Cat#161-0374
Protease inhibitor cocktail	Sigma-Aldrich	Cat#P8340
PVDF membrane	GE Healthcare	Cat#10600023
Pyridine	MP Biomedicals	Cat#0230018301
ReadyStrip IPG strips	BioRad Laboratories	Cat#163-2015
Sodium dodecyl sulfate	Fisher Scientific	Cat#BP166-5
Succinic acid, disodium	Sigma-Aldrich	Cat#224731
Succinic acid-$^{13}C_4$	Cambridge Isotope Laboratories	Cat#CLM1571
Sucrose	Sigma-Aldrich	Cat#S0389
Taxol	Cytoskeleton	Cat#TXD01

TCEP hydrochloride	Thermo Fisher Scientific	Cat#T2556
Thiamine pyrophosphate	Sigma-Aldrich	Cat#C8754
Trimethylchlorosilane	Sigma-Aldrich	Cat#386529
Tris Base	Fisher Scientific	Cat#BP152-5
Triton X-100	Sigma-Aldrich	Cat#T9284
Trypsin, mass spectrometry grade	Promega	Cat#V5280
4-Vinylpyridine	Sigma-Aldrich	Cat#V3204
Water, LC-MS grade	Fisher Scientific	Cat#W-4
Zeba Spin Columns	Thermo Scientific	Cat#89882S
Critical Commercial Assays		
Deposited Data		
http://dx.doi.org/10.17632/3y7yp7c8bj.1		
Experimental Models: Cell Lines		
N1E-115 (subclone N1E-115-1)	Sigma-Aldrich	Cat#08062511
Experimental Models: Organisms/Strains		
Mouse: *NDUFS4* $^{-/-}$	Kruse et al., 2008	RRID:MGI:4818649
Oligonucleotides		
Recombinant DNA		
Software and Algorithms		
ImageJ	Scheneider et al., 2012	https://imajej.nih.gov/ij/
GraphPad Prism 6.0	N/A	N/A
Proteome Discover 1.4	N/A	N/A
Scaffold 4D	N/A	N/A
Xcalibur 4.3	N/A	N/A
Other		

LEAD CONTACT AND MATERIALS AVAILABILITY

Further information and requests for reagents should be directed to and will be fulfilled by the Lead Contact, Norma Frizzell (norma.frizzell@uscmed.sc.edu). This study did not generate new unique reagents.

EXPERIMENTAL MODELS AND SUBJECT DETAILS

Mice

Animal care and use procedures were carried out in accordance with the National Institutes of Health Guide for the Care and Use of Laboratory Animals, and approved by The University of South Carolina Animal Care and Use Committee. Mice were housed in a pathogen-free animal facility under a 12h light/dark cycle (lights on from 7AM to 7PM) and received Teklad 8904 rodent diet and water ad libitum. Ndufs4$^{+/-}$ mice (129/Sv x C57BL/6 mixed background) from our colony, originally obtained from Drs. Richard Palmiter and Albert Quintana (Seattle Children's Research Institute, Seattle, WA) (Kruse et al., 2008; Quintana et al., 2010), were mated in trios (one male and two females), switched to a breeder's rodent diet (LabDiet 5058) and the litters were weaned at 21 days of age. Genotyping was performed as previously described (Piroli et al., 2016), and both male and female mice were used. Ndufs4$^{+/+}$ and Ndufs4$^{-/-}$ mice were sacrificed by decapitation under deep isoflurane anesthesia at 8 weeks of age. The brain was removed from the skull, and the brainstem (BS), olfactory bulbs (OB) and cerebellum were dissected. For some protocols fresh brain regions were used immediately; on other occasions the tissues were snap frozen in liquid nitrogen and stored at -80 °C until further use (see METHODS DETAILS).

N1E-115 Cells

N1E-115 cells neuroblastoma cells (subclone N1E-115-1) were expanded in non-differentiation medium containing 90% DMEM and 10% FBS, as previously described (Piroli et al., 2016; Piroli et al., 2019). At 80% confluence, the cells were differentiated into neurons in the presence of 2% FBS and 1.25% dimethyl sulfoxide in DMEM for 5 days.

METHOD DETAILS

Mouse brain preparations for immunoblotting

Considering the abundance of tubulin in brain preparations, the high level of tubulin succination, and the location of the ~48-50 kDa succinated band that we describe in this manuscript immediately below tubulin, we followed three different protocols in an attempt to enrich the preparations in the ~48-50 kDa band and at the same time deplete them of tubulin.

First, we subjected mouse BS samples to an *in vitro* tubulin polymerization protocol that we previously described (Piroli et al., 2014). Briefly, frozen mouse BS samples were reduced to a powder with a pestle in a mortar containing liquid nitrogen. The pulverized tissue was then resuspended in cold Mes/glutamate buffer (0.1 M Mes, pH 6.8, containing 0.5 mM $MgCl_2$, 1 mM EGTA, 1 M glutamate, 1 mM DTT and a protease inhibitor cocktail), in a volume ratio of 1:1.5 (powder:buffer). The suspension was pulse sonicated at 2 watts using a Model 100 sonic dismembrator (Fisher Scientific) for 5 intervals of 10 s. The total protein homogenate was then centrifuged at 30,000 x *g* at 4°C for 15 min to generate a pellet (P1) that was analyzed by immunoblotting, and the supernatant (S1) was subjected to microtubule polymerization by addition of 20 µM taxol and 1 mM GTP, followed by incubation for 30 min at 37°C.

Following further centrifugation at 30,000 x *g* for 30 min at 37°C, the supernatant of microtubules (SM) was removed, desalted through Zeba Spin Columns (MW cut-off 7 kDa, Thermo Scientific) and analyzed by immunoblotting; the microtubular pellet (MP) composed of >95% tubulin was not used.

Second, we prepared gliosomes and synaptosomes from BS and cerebellum samples according to Carney et al. (2014), with minor modifications. Briefly, fresh BS and cerebellum samples were homogenized in 0.32 M sucrose, 1 mM EDTA, 10 mM HEPES pH 7.4 using a glass-teflon homogenizer; the resulting crude homogenates were centrifuged at 1,000 x *g* at 4°C for 5 min. The supernatants (cleared homogenates) were then loaded on top of a gradient composed of layers containing 3, 7, 10 and 20% Percoll in the homogenization buffer; a fraction of the cleared homogenate was saved for immunoblotting comparative purposes. The gradients were centrifuged at 33,500 x *g* at 4°C for 6 min without brakes, and the interfaces between 3 and 7% Percoll (gliosomes), 10 and 20% (synaptosomes) and the loose pellet at the bottom of the tubes were collected and washed with the homogenization buffer to remove the Percoll. All the collected fractions and the cleared homogenates were analyzed by immunoblotting.

Third, we prepared purified mitochondrial fractions according to Kayser et al. (2016), with minor changes. Briefly, fresh BS samples were homogenized in 225 mM mannitol, 75 mM sucrose, 1 mM EGTA, 5 mM HEPES pH 7.2 containing 1 mg/ml fatty acid-free BSA and a protease inhibitor cocktail using a glass-teflon homogenizer; the resulting crude homogenates were centrifuged at 1,100 x *g* at 4°C for 2 min. The supernatants (cleared homogenates) were added Percoll to a 5% concentration, and then layered on top of 15% Percoll; a fraction of the cleared homogenate was saved for immunoblotting comparative purposes. The gradients were centrifuged at 18,500 x *g* at 4°C for 10 min; the top layer, the interface and the lower layer were removed and the loose pellets at the bottom of the tubes were collected and washed with 250 mM sucrose, 0.1 mM EGTA, 5 mM HEPES pH 7.2 to remove the Percoll. The mitochondrial pellets and the cleared homogenate were analyzed by immunoblotting.

Cell Treatments

To increase succination, N1E-115 cells were treated during the final 24 h of differentiation with 0-100 µM dimethyl fumarate (DMF) prepared in Dulbecco's PBS (DPBS) and filtered; some of the wells received dimethyl succinate (DMS) in the same range of concentrations as a negative control. The cell collection and preparation is described in detail in the section "Measurement of the α-ketoglutarate dehydrogenase complex activity".

One-dimensional PAGE and Western Blotting

Western blotting was performed as described previously (Piroli et al., 2014; Piroli et al., 2016; Piroli et al., 2019). Ten to fifty µg of proteins were run on 12% gels (Criterion, BioRad) and transferred to PVDF membranes. Immunoblotting was performed with antibodies listed in the Key Resources Table. The preparation of the polyclonal anti-2SC antibody has been described previously (Nagai et al., 2007). In most cases, membranes were stripped with 62.5 mM Tris, pH 6.8, containing 2% SDS and 0.7% 2-mercaptoethanol for 15 min at 65°C prior to reprobing. Chemiluminescent signals were captured on photographic film (HyBlot CL).

Two-dimensional Gel Electrophoresis and Western Blotting

Isoelectric focusing on pI 4-7, 11 cm strips and two-dimensional (2D) gel electrophoresis was performed in an Ettan IPGphor II device (Amersham Biosciences) as described previously (Piroli et al., 2014; Piroli et al., 2016). The 2D gels were transferred onto PVDF membranes to detect protein succination by western blotting; the blots were then stripped and subjected to DLST detection.

Measurement of the α-ketoglutarate dehydrogenase complex activity in brain regions

The activity of the α-ketoglutarate dehydrogenase complex (KGDHC) was measured by following the formation of NADH at 340 nm according to Yang et al. (2009), with minor modifications. BS and OB frozen samples were homogenized in 50 mM Tris-HCl pH 7.2 containing 1 mM dithiothreitol, 0.2 mM EGTA, 0.4% Triton X-100 and a protease inhibitor cocktail using a glass-teflon homogenizer. The crude homogenates were centrifuged at 2,000 x *g* for 4 min at 4°C; the supernatants were used to determine KGDHC activity. One hundred µl of a reaction mix containing 50 mM Tris-HCl pH 7.8, 1 mM $MgCl_2$, 1 mM $CaCl_2$, 0.5 mM EDTA, 0.3 mM thiamine pyrophosphate, 0.1% Triton X-100 and 1 mM dithiothreitol were added to the wells of a 96-well plate, followed by 50 µl of an assay mix containing 50 mM Tris-HCl pH 7.8, 3 mM NAD^+ and 0.75 mM coenzyme A, and then 25 µl of the tissue preparations containing 5-10 µg protein (or homogenization buffer for the blanks). A baseline reading every min for 10 min with the temperature set at 30°C was taken at 340 nm in a plate reader (Tecan Safire^2, TECAN Systems Inc.). After the addition of 25 µl 3 mM α-ketoglutarate in 50 mM Tris-HCl pH 7.8 (or 50 mM Tris-HCl pH 7.8 for "no substrate" controls), further readings were taken for an additional period of 60 min. The readings in the absence of α-ketoglutarate were subtracted from those in the presence of the substrate, and these corrected values were plotted as a function of time to calculate the V_{max} from the slopes. Each sample was run in triplicates that were averaged; the n size was 3-4 for each experimental group. The results were converted to mU/mg of protein considering $E_{NAD(340)}$ = 6.22 $cm^{-1}mM^{-1}$ and a path length of 0.6 cm.

Measurement of the KGDHC activity in purified bovine heart complex and N1E-115 cells

In vitro succination effects on the activity of a commercially available bovine heart KGDHC standard was studied after incubation for 18 h at room temperature with a range of 0-2 mM DMF following the protocol described above for brain regions; dithiothreitol was replaced with 300 µM tris(2-carboxyethyl) phosphine (TCEP) to avoid the possible reaction of DMF with dithiothreitol. The results of the KGDHC activity were expressed as % of the control group (no DMF added). The KGDHC activity was also measured in N1E-115 cells treated with DMF or DMS (see "Cell Treatments" above) with minor modifications. Briefly, the medium was removed; the cells were rinsed 3 times with DPBS and gently scraped with 50 mM Tris-HCl pH 7.2 containing 1 mM dithiothreitol, 0.2 mM EGTA, 0.4% Triton X-100 and a protease inhibitor cocktail. The extracts were homogenized in a glass-glass homogenizer, the resulting homogenates were centrifuged at 2,000 x *g* for 4 min at 4°C, and the supernatants were used to determine KGDHC activity following the protocol described above for brain regions. The results of the KGDHC activity were expressed as % of the control group (no DMF or DMS added).

Substrate level phosphorylation measurements

Mitochondrial isolation and measurement of ATP synthesis was performed according to Komlódi and Tretter (2017), with minor modifications. Freshly obtained BS and OB from Ndufs4 KO mice and WT littermates were immediately homogenized in 5 mM Tris pH 7.4 containing 225 mM mannitol, 75 mM sucrose and 1 mM EGTA using a glass-teflon homogenizer. The initial homogenates were centrifuged at 1,300 x *g* for 3 min, and the supernatant was further centrifuged at 20,000 x *g* for 10 min. The resultant pellet was resuspended in 15% Percoll and then layered on top of a discontinuous Percoll gradient consisting of 23% and 40% layers. The gradients were then centrifuged at 30,700 x *g* for 8 min using no brake at the end. Immunoblotting experiments determined that the interface between the 23% and 40% Percoll and the loose pellet in the 40% Percoll layer were enriched in mitochondrial markers and devoid of myelin (Figure S3A). Consequently, these two fractions were pooled together, topped with homogenization buffer and centrifuged for 10 min at 16,600 x *g*; and the pellet was re-suspended in homogenization buffer and subsequently centrifuged again for 10 min at 6,300 x *g* for 10 min. The resulting purified mitochondrial pellet was re-suspended in 5 mM Tris pH 7.4 containing 225 mM mannitol and 75 mM sucrose, and immediately used for mitochondrial ATP synthesis measurements. The assay medium consisted of 20 mM HEPES pH 7.0 containing 0.1 mM EGTA, 125 mM KCl, 2 mM K_2HPO_4, 1 $MgCl_2$, and 0.025% fatty acid-free bovine serum albumin, with the addition of 3 mM $NADP^+$, 5 mM glucose, 300 µM AP5 (P^1,P^5-Di(adenosine-5') pentaphosphate; an inhibitor of adenylate kinase), 0.75 U/ml hexokinase, and 0.25 U/ml glucose-6-phosphate dehydrogenase, in a final volume of 200 µl. ATP formation was detected through the phosphorylation of glucose by added hexokinase, coupled to the oxidation of the resulting glucose 6-phosphate by added glucose 6-phosphate dehydrogenase, with formation of NADPH. NADPH synthesis was followed at 340 nm in a plate reader as described for the measurement of α-ketoglutarate dehydrogenase complex activity (see above). Basal measurements started upon addition of the mitochondrial samples (5 µg/well) and ADP (2 mM) for 10 min at 37°C, followed by the addition of α-ketoglutarate or succinate (both at 5 mM); some wells also received oligomycin (8 µM) to determine total ATP synthesis (oxidative phosphorylation + substrate level phosphorylation) in the absence of oligomycin, and substrate level phosphorylation in the presence of oligomycin. Corrections in the absence of substrate were applied, and these corrected values were plotted as a function of time to calculate the ATP synthesis from the slopes. Each sample was run in triplicates that were averaged; the n size was 7-12 for each experimental group. The results were converted to nmoles ATP/min/mg of protein using an ATP curve (range: 0-20 nmoles). These mitochondrial fractions were also used for immunoblotting experiments (succinylation, acetylation and succination studies in Figure 4 (and Figure S3) and detection of protein lipoylation (Figure S1))

Determination of Protein Content

The protein content in all the brain and cell preparations, including samples for immunoblotting and those for the determinations of enzymatic activity was determined by the method of Lowry et al. (1951).

Metabolite Quantification

TCA cycle metabolite quantification was performed in an adaptation of previous methods (Oldham et al. 2016, Manuel et al. 2020). Metabolites were extracted by adding 1ml ice-cold 80% methanol to snap-frozen olfactory bulbs. The tissue was dissociated in pre-cooled glass-teflon homogenizers and transferred

to 1.5 ml Eppendorf tubes. Homogenized samples were briefly pulse-sonicated and frozen for 15 min at -70°C. After thawing, the samples were centrifuged at 15,000 x *g* for 10 min at 4°C. The supernatants were transferred to new Eppendorf tubes and the extracts were dried by centrifugal evaporation. The protein pellet was resuspended in RIPA buffer for quantification by the Lowry method.

The quantification of L-lactate by LC-MS was performed following chiral derivatization with diacetyl-L-tartaric anhydride (DATAN). 50 µM L-lactate-$^{13}C_3$ internal standard was added to tissues prior to extraction, and to all racemic lactate standards. Dried tissue metabolite extracts and standards were resuspended in 50 µl DATAN prepared in acetonitrile:acetic acid (4:1, v/v) to 50 mg/ml and heated to 70 °C for 2 h. The samples were cooled to room temperature and centrifuged at 1000 X *g* for 5 min. The derivatized samples were further diluted to 100 µl with acetonitrile, vortexed, and transferred to LC vials for analysis. LC separation was performed on Thermo Vanquish Flex liquid chromatograph using a PEEK coated SeQuant ZIC HILIC column (Merck Millipore). The column was 2.1 mm x 150 mm with 3.5 µm particles and was preceded by an equivalent 20 mm long guard column. 1 µl of sample was separated by isocratic elution with 15% mobile phase A (10% 200 mM formic acid:90% LC-MS grade water) and 85% mobile phase B (10% 200 mM formic acid:90% acetonitrile) at a total flow rate of 200 µl/min. The formic acid was titrated to pH 3.25 with ammonium hydroxide. Negative ion electrospray mass spectra were acquired on a Thermo Q-Exactive HF-X quadrupole-Orbitrap in MS/MS mode with the Orbitrap resolution set at 7,500. Precursor ions (305 or 308 Da) were isolated by the quadrupoles and fragmented in the HCD cell at 10 ev. The product ions were mass analyzed in the Orbitrap. XCalibur 4.3 software was used to construct chromatograms of the transitions 305>89 (lactate) and 308>92 (L-lactate-$^{13}C_3$). The areas of the lactate peaks were normalized to the areas of the ^{13}C internal standard.

The quantification of TCA cycle intermediates was performed by GC-MS at the David H. Murdock Research Institute (DHMRI, Kannapolis, NC). Prior to derivatization the extracts were resuspended in ethyl acetate and transferred to GC-MS vials. The samples were dried with N_2, and an internal standard (100 µM succinate-$^{13}C_4$) was added to each of the samples and standards. The samples and standards were derivatized with 200 µl of methylamine (20 mg/ml in pyridine) at 30°C for 90 min, followed by drying under N_2. This was followed by the addition of 120 µl of N-methyl-N-(trimethylsilyl) trifluoroacetamide (MSTFA) with 1% trimethylchlorosilane (TMCS); the mixture was incubated at 70°C for 60 min. The derivatized product was stored in a -20°C freezer for one hour prior to GC/MS analysis. An Agilent 7890A GC system, coupled to an Agilent 5975C electron ionization (EI) mass selective detector (MSD) was used to analyze the TMS-derivatized samples. Select ion monitoring (SIM) was performed and the peak areas obtained were normalized to the internal standard. Absolute quantitation for all metabolites was performed based on standard curves obtained from the normalized reference standards, and the final metabolite concentrations were normalized to tissue weights or total protein content.

Protein identification by liquid chromatography-tandem mass spectrometry (LC-MS/MS)

The in-gel protein digestion method used was previously described (Piroli et al., 2016; Piroli et al., 2019). Briefly, samples of the pellets obtained from the synaptosomal preparations (20 µg of protein) were resolved by SDS-PAGE in 7.5% gels; the gels were stained with Coomassie Brilliant Blue and the bands of interest in the ~48-50 kDa region were excised. The gel pieces were destained, washed with 50 mM

ammonium bicarbonate in 50% acetonitrile, and dehydrated with 100% acetonitrile; proteins were then reduced with 10 mM dithiothreitol and alkylated with 170 mM 4-vinylpyridine. Protein digestion was carried out overnight at 37°C in the presence of 500 ng sequencing grade modified trypsin in 50 mM ammonium bicarbonate. After gel extraction with 5% formic acid in 50% acetonitrile, the samples were analyzed in a blinded manner on a Dionex Ultimate 3000-LC system (Thermo Scientific) coupled to a Velos Pro Orbitrap mass spectrometer (Thermo Scientific). The LC solvents were 2 % acetonitrile/0.1 % formic acid (Solvent A) and 80 % acetonitrile/0.1 % formic acid (Solvent B); the water used for these solvents was LC-MS grade. Peptides were first trapped on a 2 cm Acclaim PepMap-100 column (Thermo Scientific) with Solvent A at 3 µl/min. At 4 min the trap column was placed in line with the analytical column, a 75 µm C18 stationary-phase LC PicoChip Nanospray column (New Objective). The peptides were eluted with a gradient from 98%A:2%B to 40%A:60%B over 30 min, followed by a 5 min ramp to 10%A:90%B that was held for 10 min. The Orbitrap was operated in data-dependent acquisition MS/MS analysis mode and excluded all ions below 200 counts. Following a survey scan (MS1), up to 8 precursor ions were selected for MS/MS analysis. All spectra were obtained in the Orbitrap at 7500 resolution. The DDA data were analyzed using Proteome Discover 1.4 software with SEQUEST algorithm against the uniprot_ref_mouse database (2014-10-03 version, 52,474 proteins) with XCorr validation >2 (+2) or >2.5 (+3). An allowance was made for 2 missed cleavages following trypsin digestion. No fixed modifications were considered. The variable modifications of methionine oxidation (M^{OX}), proline hydroxylation (P^{OX}), cysteine pyridylethylation (C^{PE}, 105.058) or cysteine succination by fumarate (C^{2SC}, 116.011) were considered with a mass tolerance of 15 ppm for precursor ions and a mass tolerance of 10 ppm for fragment ions. The results were filtered with a false discovery rate of 0.01. For all DLST peptides identified the spectra were manually inspected to confirm the abundance of product ions. The software Scaffold 4D was used to generate the spectrum in Figure 1D.

QUANTIFICATION AND STATISTICAL ANALYSIS

Results were expressed as means ± standard error of the mean (SEM). For the enzymatic activities, a description of the calculations is presented in the corresponding subheading under METHOD DETAILS. Statistical comparisons between two experimental groups were performed using unpaired *t* tests; when three or more groups were compared, one-way ANOVA followed by Student-Neuman-Keuls' test was applied. The n size for each particular experiment is shown in the Figures, and represents the number of individual biological replicates. Differences were considered statistically significant when a P value < 0.05 was achieved. The software Image J (NIH) was used for the quantification of band intensities by densitometry (Tanis et al., 2015). The software GraphPad Prism V6.0 was used for statistical analysis and graphs.

DATA AND CODE AVAILABILITY

The mass spectrometry .RAW files used to identify dihydrolipoyllysine-residue succinyltransferase peptides have been deposited in Mendeley Data with the identifier:

http://dx.doi.org/10.17632/3y7yp7c8bj.1

Supplemental Material

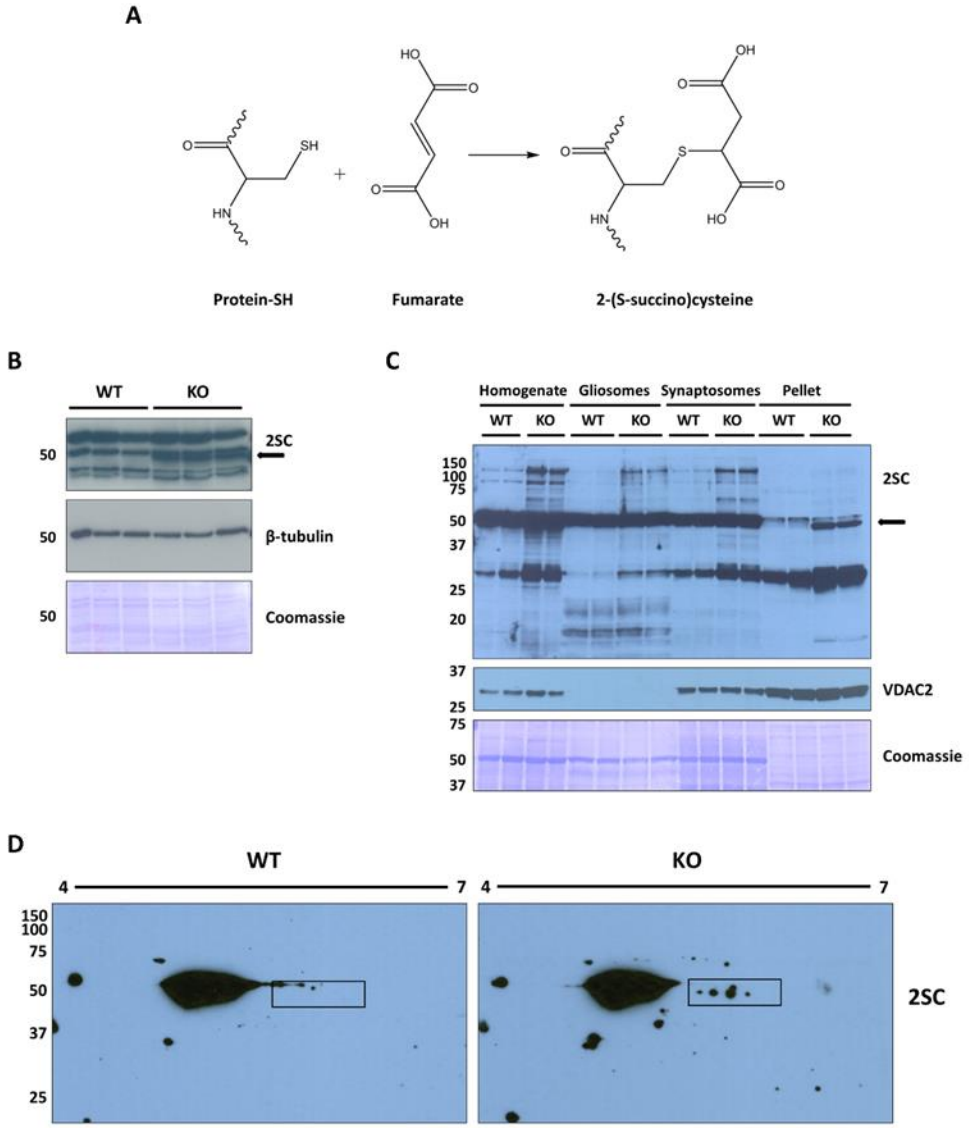

Figure S1: A band at ~48-50 kDa is differentially succinated in the BS and CB of the Ndufs4 KO mouse.

A, Formation of 2-(S-succino)cysteine (2SC) by reaction of fumarate with cysteine residues in proteins. *B*, Detection of a distinct succinated band at ~48-50 kDa (arrow) in a supernatant obtained after high speed centrifugation of *in vitro* polymerized microtubules from Ndufs4 KO BS homogenates. Tubulin and Coomassie panels show even load of proteins (30 µg prot/lane). *C*, The cerebellum (CB) also shows some

evidence of neuropathology in the KO mice. Similar to the BS (see Figure 1B), a band at ~48-50 kDa shows increased succination in a pellet fraction after synapotosomal and gliosomal preparation of the cerebellum (CB) of Ndufs4 KO mice (arrow in 2SC panel). The pellets are enriched in the mitochondrial marker VDAC2. Coomassie panel shows even protein load (15 µg prot/lane) within each fraction group. *D*, Similar to BS (see Figure 1E), a train of succinated spots is observed in the region of ~48-50 kDa and pH 5.5-6.3 (rectangular area) in Ndufs4 KO mice CB preparations. In *A*-*D*, molecular weight markers are shown on the left side.

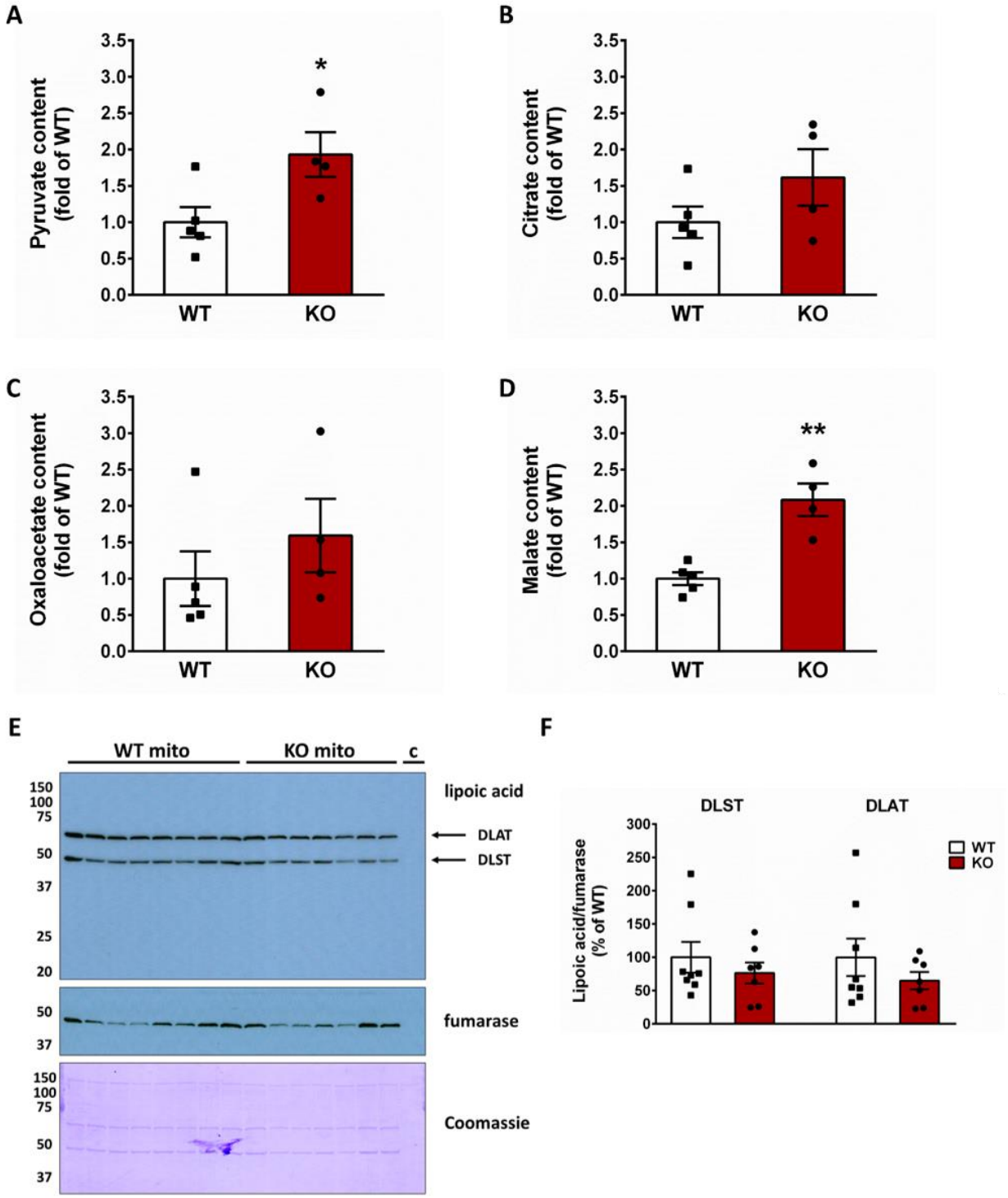

Figure S2: Select TCA cycle metabolites are increased in the Ndufs4 KO brain

A-D, Pyruvate (*A*), citrate (*B*), oxaloacetate (*C*), and malate (*D*) contents in the OB of Ndufs4 KO and WT mice. E, Detection of lipoic acid moieties associated with DLST and DLAT (dihydrolipoyllysine-residue

acetyltransferase, a component of the pyruvate dehydrogenase complex) in the BS of WT and Ndufs4 KO mice. In addition to the mitochondrial fractions ("mito"), a lane with a cytosolic preparation ("c") was included as a negative control. *F,* Quantification of the blots in *E*, relative to fumarase. In *F,* results expressed as means ± SEM were compared by unpaired t test (NS). In *A*-*D*, molecular weight markers are shown on the left side.

Results are expressed as means ± SEM. Comparisons by unpaired t test (* $p<0.05$, ** $p<0.01$ vs. WT).

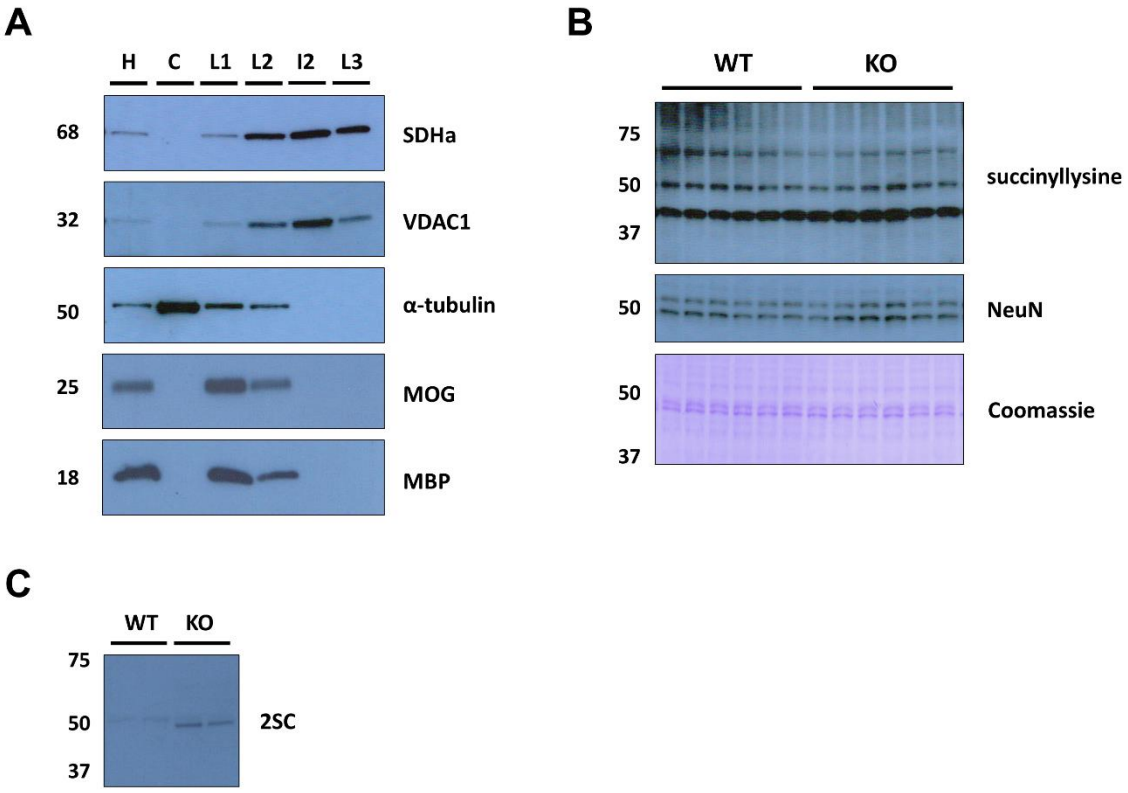

Figure S3: Characterization of the different fractions obtained during mitochondrial preparation for SLP measurements

A, The initial homogenate (H), cytosol (C), and different fractions obtained after separation of the initial particulate pellet through a Percoll density gradient, including layer 1 (L1), layer 2 (L2), interface 2 (I2) and layer 3 (L3) were separated by SDS-PAGE. After protein transfer the mitochondrial markers (SDHa and VDAC1), cytosolic markers (α-tubulin) and myelin markers (MOG and MBP) were detected by immunoblot. Fractions I2 and L3 were combined for the SLP assay due to enrichment of mitochondria and lack of cytosol components and myelin.

B, Protein succinylation is not affected in nuclear fractions obtained from the BS of Ndufs4 KO mice, NeuN (nuclear marker) and Coomasie were used as loading controls.

C, Confirmation that succination of a band at ~48-50 kDa in mitochondrial fractions from BS is limited to Ndufs4 KO mice.

Table S1: MS/MS peptide identification for dihydrolipoyllisine-residue succinyltransferase component of 2-oxoglutarate dehydrogenase complex. Raw data were searched with the Sequest HT node of Proteome Discover 1.4 (SP1), using the uniprot_ref_mouse database. Variable modifications of methionine oxidation (M^{OX}), proline oxidation (P^{OX}), cysteine pyridylethylation (C^{PE}), and cysteine succination by fumarate (C^{2SC}) were considered. The peptides identified are reported from 3 individual KO mice analyzed.

Swiss-Prot Accession #	Protein Identity	% Coverage	Peptides Identified	PSMs	M+ (Da)	Charge
Q9D2G2	Dihydrolipoyllisine-residue succinyltransferase component of 2-oxoglutarate dehydrogenase complex (DLST) (*Mus musculus*)	31.87	VEVRP^{OX}M^{OX}MYVALTYDHR	42	2011.97898	3
			ASAFALQEQPVVNAVIDDATK	12	2187.14591	3
			LGFM^{OX}SAFVK	9	1015.53142	2
			VEGGTPLFTLR	9	1189.66350	2
			NVETM^{OX}NYADIER	8	1470.65727	2
			NVETMNYADIER	1	1454.66118	2
			DYIDISVAVATPR	8	1419.75774	2
			TINELGEK	6	903.48235	2
			NDVITVQTPAFAESVTEGDVR	6	2248.11650	2
			AKPAETPAPAHK	3	1217.66919	3